AGU100 ADVANCING EARTH AND SPACE SCIENCE

JGR

Journal of Geophysical Research: Atmospheres

RESEARCH ARTICLE
10.1029/2017JD028116

Special Section:
East Asian Study of Tropospheric Aerosols and Impact on Cloud and Precipitation

Retrieval of Aerosol Optical Depth From INSAT-3D Imager Over Asian Landmass and Adjoining Ocean: Retrieval Uncertainty and Validation

Manoj K. Mishra[1]

[1]Space Applications Centre, Indian Space Research Organization, Ahmedabad, India

Key Points:
- An AOD retrieval algorithm is developed for the use of INSAT-3D visible band data, and theoretical uncertainty of algorithm is presented
- Validation with AERONET covering >3,500 data points shows uncertainty within theoretical limit
- Comparison with MODIS-aqua aerosol product shows good agreement

Correspondence to:
M. K. Mishra,
manoj8187@sac.isro.gov.in

Citation:
Mishra, M. K. (2018). Retrieval of aerosol optical depth from INSAT-3D imager over Asian landmass and adjoining ocean: Retrieval uncertainty and validation. *Journal of Geophysical Research: Atmospheres*, *123*, 5484–5508. https://doi.org/10.1029/2017JD028116

Received 26 NOV 2017
Accepted 26 APR 2018
Accepted article online 5 MAY 2018
Published online 24 MAY 2018

Abstract An algorithm for aerosol optical depth (τ) retrieval from imager data onboard geostationary Indian National Satellite (INSAT-3D) is described. The basic principles of the algorithm are adopted from Geostationary Observational Environmental Satellite Aerosol and Smoke Algorithm, where darkest observations over a time period and constant background aerosol optical depth (τ_b) value are used to derive surface reflectance. However, in INSAT-3D algorithm spatially and temporally dynamic τ_b derived from Moderate Resolution Imaging Spectroradiometer (MODIS)-aqua is used. The theoretical simulations suggest retrieval uncertainty of around ±30–45% depending on the certainty of aerosol optical properties and other parameters used in radiative transfer calculations. Retrieval uncertainty is less over dark regions and lower scattering angles. INSAT-3D τ at 0.55 μm is derived operationally for the first time over Asia and adjoining ocean at 30-min temporal resolution. The retrieval algorithm is validated against in situ Sun-sky radiometer measurements at 26 Aerosol Robotic Network sites and Sun-photometer measurements during Sagar-Sampada cruise in the northern Arabian Sea. The validation study encompassing 3,803 and 844 data points over land and ocean stations show correlations ranging from 0.70 to 0.91 and 0.79 to 0.91, respectively. The uncertainty of retrievals is within 45% over land and within 30% over ocean. The diurnal variability of INSAT-3D and Aerosol Robotic Network τ in India and southeast Asia is also presented. The comparison of INSAT-3D and MODIS-aqua monthly average τ shows correlation ranging from 0.74 to 0.89 and 0.65 to 0.97 over Indian landmass and adjoining ocean, respectively. The validation suggests that INSAT-3D can be used for aerosol monitoring and can be merged with MODIS-aqua/terra aerosol product to generate combined aerosol product at high temporal resolution.

1. Introduction

Aerosol affects Earth's radiation budget directly by changing the radiation reflected from the Earth surface as well as by altering the incoming solar radiation. They can also affect Earth's radiation budget indirectly by changing the cloud properties (Intergovernmental Panel on Climate Change, 2007). Since aerosol plays a major role in cloud condensation, therefore, it also shows an impact on precipitation. Increasing interests in understanding the role of aerosol in radiative forcing and climate change require monitoring of the global distribution of aerosols. Moreover, the impact of aerosol on air quality (in other words impact of aerosol on human health) requires accurate measurements of aerosol optical depth (AOD) τ and aerosol properties at high temporal resolution (Pope, 2000). Number of networks such as Aerosol Robotic Network (AERONET) and ISRO Geosphere-Biosphere Programme acquires continuous ground observation of AOD and aerosol properties around the world at very high temporal resolution (Holben et al., 1998; ISRO-Geosphere-Biosphere Programme, 2017). However, aerosols are very dynamic spatially as well as temporally; therefore, point observations from these networks do not represent the real spatial distribution of AOD and their optical properties. In Asian standpoint, recent reports (Intergovernmental Panel on Climate Change, 2007) about severely elevated air pollution in metropolitan cities, located in developing countries of Asia such as India and China, led to an urgency of synoptic measurement of AOD over Asian landmass at high temporal resolution to understand the possible causes such as transportation of aerosol from other places and anthropogenic activities and to identify hotspots of aerosol sources. Currently, satellite data are leading source for synoptic representation of AOD. The aerosol retrievals from instruments onboard polar orbiting satellites such as Moderate Resolution Imaging Spectroradiometer (MODIS) and Multi-angle Imaging SpactroRadiometer provide valuable and accurate global estimates of AOD over land and oceans (Hsu et al., 2004, 2006, 2013; Kaufman et al., 1997; Levy et al., 2007). However, aerosol retrievals from polar

satellites are limited in temporal resolution (once a day); therefore, it may not be perfect for monitoring the aerosol motion especially in countries such as India and China where aerosols do not exhibit a systematic diurnal trend (Kaufman et al., 2000) due to high anthropogenic and dust activities. On the other hand, the frequent measurement of AOD in time may provide useful information on aerosol emissions and transport from strong sources (e.g., dust storms and biomass burning). Geostationary satellites provide better prospects to derive aerosol information over a fixed area on Earth at high temporal resolution (at 15- to 30-min interval during sunlight time) and thus enable us to monitor the aerosol transportation and major emission sources (Choi et al., 2016; Kim et al., 2008, 2014; Wang et al., 2003; Zhang et al., 2011). By combining the accurate aerosol estimates from polar orbiting satellites and aerosol estimates at high temporal resolution from geostationary platforms will be very beneficial in our understanding of aerosol distribution, emission, and transportation, which will in turn help us to understand the aerosol impact on climate and air quality. The two operational Geostationary Observational Environmental Satellite (GOES) positioned to view the West Coast of the United States and Pacific Ocean (GOES-West) and the east coast and Atlantic Ocean (GOES-East) provide aerosol information over view coverage of 150°W to 0°E and 75°N to 75°S. However, observation of aerosol over Asian landmass and the Indian Ocean is still limited to polar orbiting satellites only. Over Asian landmass and adjoining oceanic region, the Indian National Satellite (INSAT)-3D imager onboard INSAT-3D is providing the continuous data in six spectral bands falling in visible to thermal infrared wavelengths from geostationary platform since 2013. The availability of data from the single visible channel of INSAT-3D Imager provides an opportunity to derive aerosol information over Asian land mass and Indian Ocean and thus may fulfill the gap of aerosol measurements at high temporal resolution in this critically important region in terms of aerosol abundance.

In this paper, adopting the legacy of GOES AOD algorithm (Knapp et al., 2002), we developed INSAT-3D aerosol retrieval (INSAT-3D AOD) algorithm and showed the potential of deriving the AOD from INSAT-3D visible channel data by validating the retrievals with Sun-sky radiometer measurements over land and ocean regions. The possible uncertainty in INSAT-3D aerosol retrieval is described and worked out on the basis of radiative transfer (RT) simulations. We also compared INSAT-3D and MODIS-aqua AOD retrievals to explore the feasibility of using combined polar and INSAT-3D AOD retrievals for the climatological study of Earth over Asian landmass and Indian Ocean. The GOES-AOD algorithm uses the fixed viewing geometries of GOES to derive surface reflectance from atmospherically corrected darkest observation over a period of time which is then used to retrieve near-real-time AOD. In GOES-AOD a fixed value of background AOD τ_b is used for correcting the darkest observation to derive surface reflectance ρ_s. A similar approach is used in INSAT-3D AOD algorithm but with the dynamic value of τ_b due to high aerosol loading and high seasonal and geographical variability of AOD over Asian countries. The aerosol product from INSAT-3D described here has been made operational on MOSDAC and VEDAS which can be freely downloaded from MOSDAC/ISRO website (https://vedas.sac.gov.in/vedas/; www.mosdac.gov.in/). The detailed description of retrieval method is given in the next section followed by an uncertainty analysis of the retrieval. The INSAT-3D AOD algorithm is then validated against surface observations and compared to the monthly average of AOD retrievals from MODIS-aqua over Indian landmass and Arabian Sea and Bay of Bengal (BOB) region. The diurnal variability of INSAT-3D and AERONET AOD in India and Southeast Asia is also presented.

2. INSAT-3D Aerosol Retrieval Method

INSAT-3D imager is a multispectral radiometer capable of generating the images of the Earth in six wavelength bands significant for metrological observations, namely, visible, shortwave infrared, middle infrared, water vapor (WV), and thermal infrared 1 and thermal infrared 2 regions (INSAT-3D ATBD, 2015; Patel et al., 2016). The central wavelengths of visible, shortwave infrared, middle infrared, WV, thermal infrared 1, and thermal infrared 2 are, respectively, 0.65, 1.62, 3.9, 6.8, 10.8, and 12.0 μm. The spectral response function of INSAT-3D Imager channels can be found at https://satellite.imd.gov.in/dynamic/INSATSRF.pdf. The INSAT-3D AOD uses the visible channel of INSAT-3D Imager instrument (0.50–0.80 μm) to retrieve aerosol information. The actual resolution of this channel is 1×1 km^2 at nadir, and data are available at up to 30-min intervals. The INSAT-3D data are binned at 10×10-km^2 resolution after cloud masking (see section 2.2.1) to improve the signal-to-noise ratio to the required value. The study about the calibration of INSAT-3D Imager in Patel et al. (2016) shows that the visible channel radiance data are well calibrated within an uncertainty of 0.5%.

Table 1
Aerosol Model Characteristics Adopted From Different Sources Used in INSAT-AOD Algorithm and in Uncertainty Analysis

Aerosol model	Mode	r_m μm	σ	f_i	$m_{i,\ real}$	$m_{i,\ img}$	Source
Rural	Water soluble	0.005	2.99	0.938299	1.53	5E−3	Lenoble and Brogniez (1984),
	Dust like	0.500	2.99	2.26490E−6	1.53	8E−3	d'Almeida et al. (1991), WMO-WCP112
	Soot	0.0118	2.00	0.0616987	1.75	0.45	
Urban	Water soluble	0.005	2.99	0.592507	1.53	5E−3	Lenoble and Brogniez (1984),
	Dust like	0.500	2.99	1.65125E−7	1.53	8E−3	d'Almeida et al. (1991), WMO-WCP112
	Soot	0.0118	2.00	0.407492	1.75	0.45	
Dust	Mode 1	0.001	2.12	0. 5421	1.53	8E−3	Kaufman et al. (1997), WMO-WCP112
	Mode 2	0.0218	3.19	0. 4579	1.53	8E−3	
	Mode 3	6.24	1.89	3.8608E−07	1.53	8E−3	
Biomass burning	Accumulation	0.0861	1.51	0.9988	1.51	0.02	Dubovik et al. (2002)
	Coarse	0.7080	2.14	0.1.2E−3	1.51	0.02	
Maritime	Water soluble	0.005	2.99	0.999579	1.53	5E−3	Lenoble and Brogniez (1984),
	Oceanic (salt)	0.300	2.51	4.20823E−4	1.38	4E−9	d'Almeida et al. (1991), WMO-WCP112

2.1. RT Model

In the INSAT-3D AOD algorithm, Second Simulation of a Satellite Signal in the Solar Spectrum-Vector (6SV) RT model has been used to simulate ρ^*_{sat} the top-of-atmosphere apparent reflectance at satellite level (Vermote et al., 1997, 2006). The 6SV is a basic RT model which is widely used and extensively validated (Kotchenova et al., 2006; Kotchenova & Vermote, 2007). It is based on the method of successive orders of scattering approximations and enables accurate modeling of satellite-level observations accounting for elevated targets, realistic molecular plus aerosol-mixed atmosphere, gaseous absorption, and Lambertian as well as anisotropic surfaces. The ρ^*_{sat} are computed assuming tropical atmosphere in the range of 0.5–0.8 μm at the spectral resolution of 0.0025 μm which are then convoluted with INSAT-3D spectral response function to simulate ρ^*_{sat} observations. The INSAT-3D visible channel is little affected by ozone and total precipitable WV (tpw) absorption for which climatological values have been used as a function of location and day of the year to simulate gaseous transmittance in the visible channel. The radiative scattering due to aerosols is simulated assuming five aerosol models defined as rural, urban, biomass burning, dust, and maritime. All five aerosol models are used for uncertainty analysis; however, for retrieval fixed rural and maritime models are used over land and ocean regions, respectively. Unlike other sensors such as MODIS where multiple visible channels are present, the INSAT-3D has only one visible channel; therefore, it is not possible to select best suited aerosol model. For this reason, the fixed aerosol model is used for retrieval. For computing the optical properties (extinction and scattering coefficients, single scattering albedo, phase function, and asymmetry factor) of these aerosol models, the optical properties of the basic modes (accumulation and coarse modes) computed from the Mie theory are mixed assuming multimodal log-normal distribution defined by

$$n(r) = \sum_{i=1}^{N} \frac{f_i}{r ln\sigma_i} \exp\left[\frac{ln^2 r/r_{m,i}}{2ln^2\sigma_i}\right] \quad (1)$$

where N is the number of modes, r is the particle radius, $r_{m,\ i}$ is the mean radius of mode i, σ_i is the width of mode i, and f_i is the number density of mode i. These parameters and the refractive index ($m_i = m_{i,\ real} + m_{i,\ img}$) for each mode used in Mie calculations are provided in Table 1. An exponential profile of AOD with scaled height of 2 km is assumed. To avoid the online RT simulation while operational retrieval of AOD, the lookup tables (LUTs) are generated using 6SV code which is used to calculate the ρ^*_{sat} as a function of solar zenith θ_o; sensor zenith θ; relative azimuth angle $\Delta\phi$, ρ_s; and AOD (varied from 0 to 2.5). The present algorithm is not intended for aerosol retrieval over glint-contaminated ocean pixels; therefore, flat surface is assumed (wind speed = 0) while computing LUTs for ocean. Eight LUTs corresponding to AOD = 0, 0.25, 0.5, 0.75, 1.0, 1.5, 2.0, 2.5 at 0.55 μm are generated for path reflectance required to estimate ρ^*_{sat}. Each LUT contains calculated path reflectance for 10 θ_o and θ values ranging from 0.0 to 72 with interval of 6° and for 16 $\Delta\phi$ values ranging from 0 to 180 with interval of 12°. Upward and downward transmittance is calculated for given θ_o and θ values for each value of AOD. Finally, eight values of spherical albedo corresponding to eight values of AOD are also tabulated.

2.2. The INSAT-3D AOD Retrieval Algorithm

The INSAT-3D AOD algorithm involves three steps: (1) generation of the clear composite image (CCI), (2) atmospheric correction of CCI to derive ρ_s, and (3) the retrieval of AOD are described in the next subsections in detail.

2.2.1. Generation of CCI

Top-of-atmosphere (TOA) apparent reflectance images $\rho_{sat} = (\pi L_{sat})/(F_o \cos \theta_o)$ are generated for previous 30 days using georeferenced visible channel data for every INSAT-3D observation time at 0600, 0630, 0700, 0730, 0800, and 0830 hr UTC. Here L_{sat} is sensor-measured radiance and F_o is the Earth-Sun distance-corrected extraterrestrial irradiance calculated for INSAT-3D visible channel. TOA reflectance images are then cloud masked. Clouds are generally characterized by higher reflectance and lower temperature than the underlying Earth surface. Threshold tests on visible channel reflectance and on infrared brightness temperature perform well for screening the thick clouds; however, these tests frequently fail when applied to thin clouds or at the edges of the clouds, which are relatively inhomogeneous than the underlying Earth surface (Martins et al., 2002). Therefore, for cloud masking the threshold test on visible channel reflectance (ρ_{sat}) and thermal channel brightness temperature (BT_{TIR}), combined with spatial variability test on visible channel reflectance is used (Martins et al., 2002). For spatial variability test, the standard deviation ($\sigma_{\rho_{sat}}$) in a marching window of 3×3 pixels is calculated and if $\sigma_{\rho_{sat}}$ exceeds certain threshold all pixels in window are identified as cloudy. Equations (2) and (3) show the threshold used in present work for cloud masking over land and ocean, respectively.

$$\text{Land}: \rho_{sat} > 0.3 \text{ or } BT_{TIR} < 273 \text{ K or } \sigma_{\rho_{sat}} > 0.02 \quad (\text{cloudy}) \tag{2}$$

$$\text{Ocean}: \rho_{sat} > 0.15 \text{ or } BT_{TIR} < 273 \text{ K or } \sigma_{\rho_{sat}} > 0.01 \quad (\text{cloudy}) \tag{3}$$

The cloud-masked images obtained for previous 30 days are then searched to find the second minimum of ρ_{sat} value for each pixel to generate ρ_{min} image, that is, the CCI for every satellite observation time. The CCI image is then binned at 10×10-km^2 resolution. The search width of window is somewhat subjective and depends on the temporal variability of atmosphere and surface reflectance in the region of interest. Ideally the width of the search window must be determined by obtaining the sufficient cloud- and aerosol-free observations in a time range with minimum variation of surface reflectance. In Indian subcontinent the surface reflectance over vegetated region varies rapidly during Rabi (December to March) and Karif cropping season (July to October); therefore, too long search window of ≥45 days will introduce a significant negative bias in derived surface reflectance. On the other hand, too small window of 15 days will make surface reflectance positively biased in regions with persistent pollution such as in Indo-Gangetic (IG) plain and parts of China and Southeast Asia. Based on the region of interest, the search window ranging from 20 to 60 days was used by various authors (Kim et al., 2008; Knapp et al., 2002, 2005). However, for operational implementation of algorithm over a large region a compromised search window of constant width must be used. In operational GOES-AOD algorithm a window of 28 days is used. Based on the operational requirement, our experience by number of iterations over Indian region and the results reported by various authors (Kim et al., 2008; Knapp et al., 2002, 2005), the search window of 30 days is currently used in operational INSAT-3D AOD algorithm.

2.2.2. Surface Reflectance Derivation

In this step, the ρ_{min} image is corrected for molecular and background aerosol scattering effects to derive ρ_s. The basic assumption in GOES-AOD (Knapp et al., 2002) and therefore in the INSAT-3D AOD algorithm is that ρ_{min} image provides the sensor measurements with minimum effect of aerosol (i.e., the clearest atmospheric condition in previous 30 days in terms of AOD). In GOES-AOD a constant value of $\tau_b = 0.04$ is used for each pixel in the image to derive ρ_s image, which generally does not hold good for the view coverage of INSAT-3D (Asian countries), especially in South Asian countries and China where some regions show persistent haziness due to pollution with AOD much higher than 0.05. Figure 1 shows the τ_b composite map for the month of December-January-February, March-April-May, and September-October-November derived by minimizing MODIS-aqua aerosol Level-2 (10-km) product for years 2013–2015. For generating τ_b composite map, the MODIS-aqua aerosol retrievals with "good" and "very good" quality, that is, with quality flag equal to 2 and 3 are used. To collocate the MODIS aerosol retrievals with INSAT-3D footprint, the INSAT-3D static latitude/longitude grid is used. Each grid box extent is then used for searching the belonging MODIS-aqua

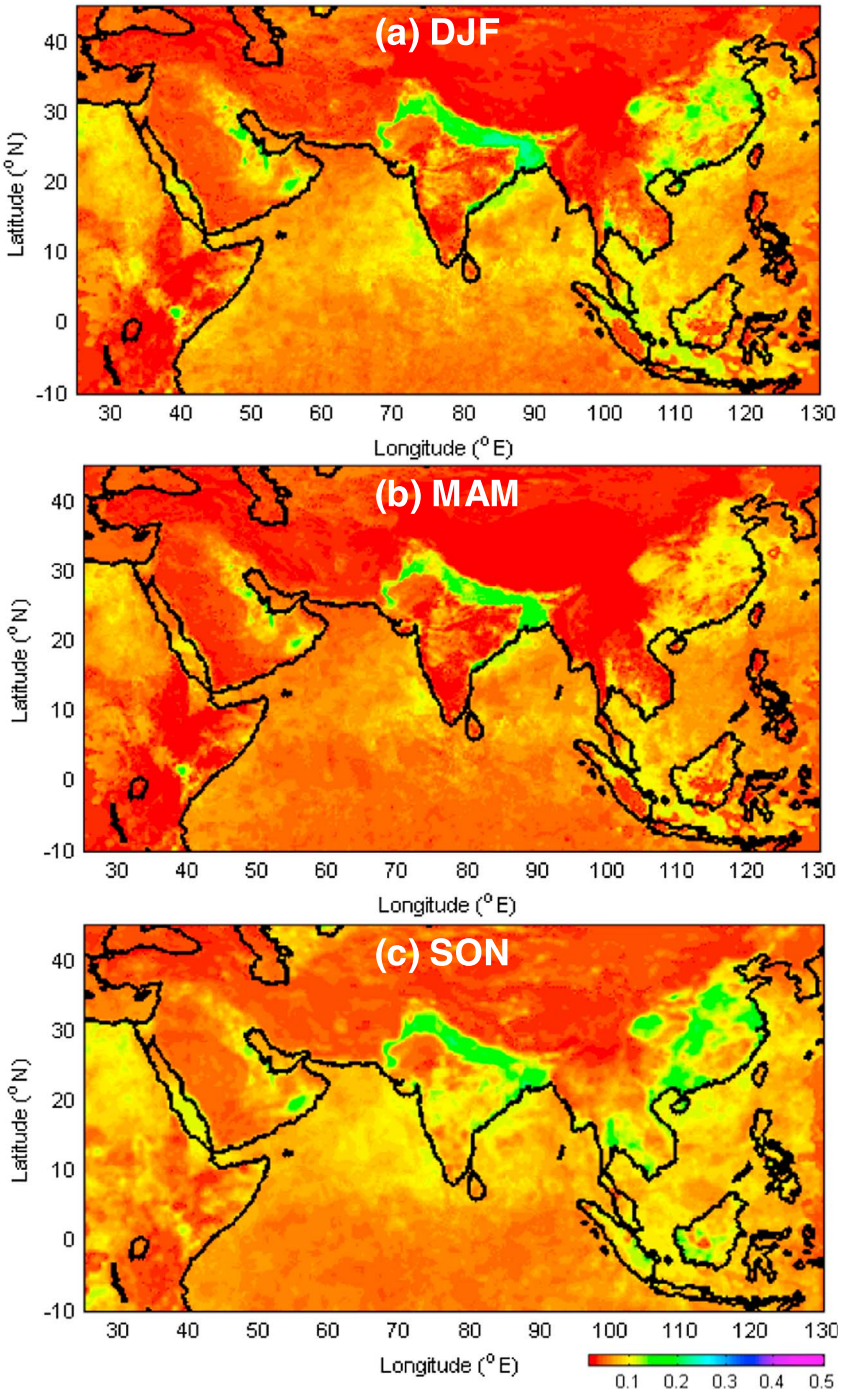

Figure 1. The background aerosol optical depth (τ_b) maps (at 10-km resolution) for (a) December-January-February, (b) March-April-May, and (c) September-October-November (SON), derived from MODIS-aqua dark target and deep blue combined aerosol product during 2013 and 2015. MODIS = Moderate Resolution Imaging Spectroradiometer; DJF = December-January-February; MAM = March-April-May; SON = September-October-November.

aerosol retrieval giving the collocated MODIS aerosol image for each day. The average of minimum 5% MODIS AOD values is selected as background AOD. From Figure 1, it is clearly seen that in regions such as India (particularly in IG plains), other Southeast Asian countries and China show elevated background aerosol conditions with $\tau_b \geq 0.1$. Moreover, significant temporal change in τ_b is observed in these regions. To account for such high τ_b conditions and their spatial and temporal heterogeneity, we used MODIS-aqua aerosol product for years 2013–2015 to generate climatological data of τ_b by searching monthly minimum value of

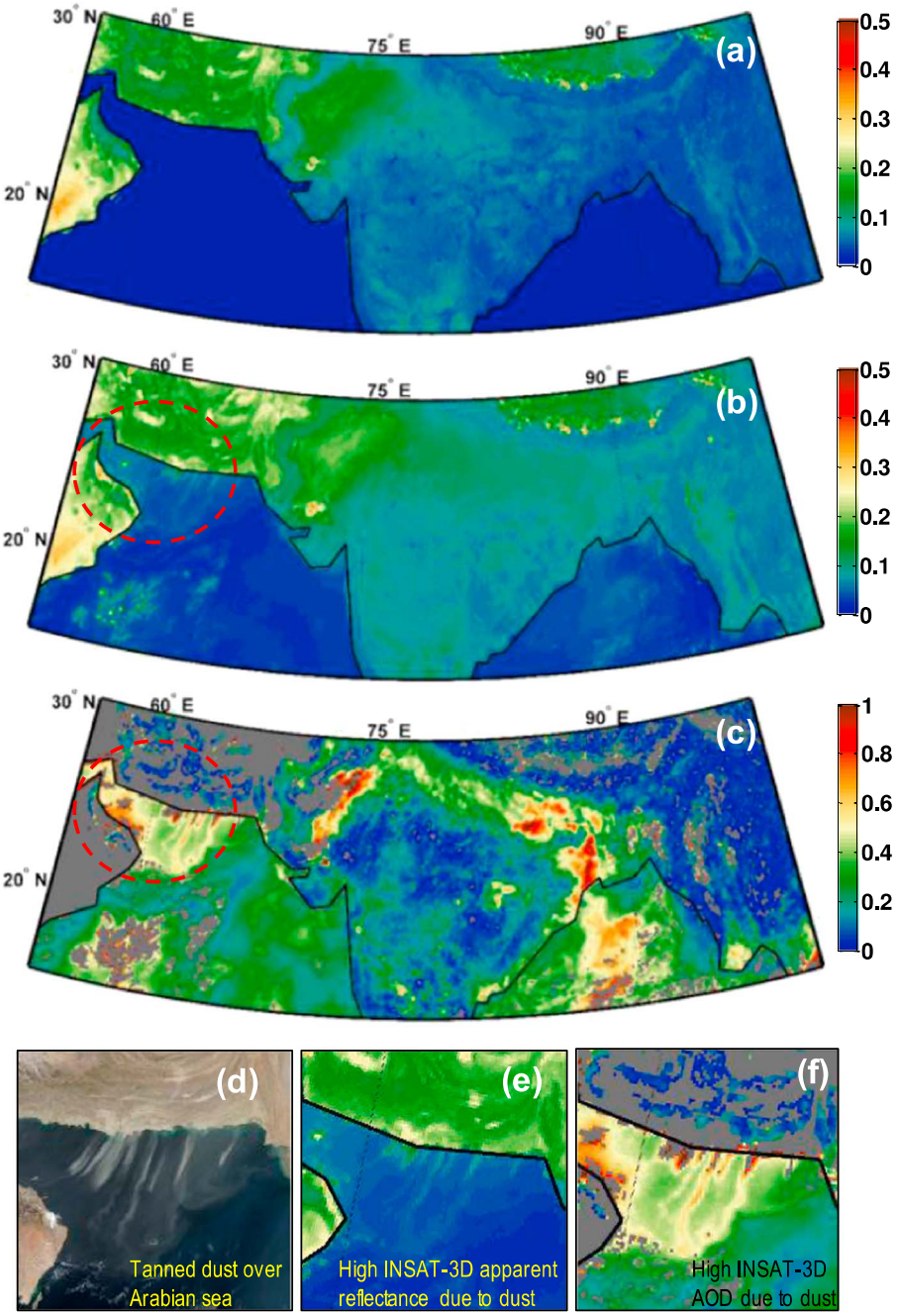

Figure 2. (a) Surface reflectance derived from INSAT-3D clear composite image over the parts of Indian subcontinent countries and adjoining ocean on 22 November 2016. (b) INSAT-3D top of the atmosphere apparent reflectance on 22 November 2016. The red circle shows the region with high apparent reflectance over dark water surface of the Arabian Sea. (c) INSAT-3D-retrieved aerosol optical depths (AODs) on 22 November 2016. (d) MODIS-aqua true color image acquired on 22 November 2016 corresponding to the region represented by the red circle in (b) and (c). This image clearly shows heavy tanned dust blown from Pakistan-Iran border toward the Arabian Sea. (e) Same as (d) but INSAT-3D apparent reflectance. The image clearly shows high apparent reflectance over dark ocean surface due to scattering from dust particles in the atmosphere. (f) Same as (d) but INSAT-3D AOD. INSAT-3D = Indian National Satellite.

AOD. These monthly τ_b maps are used for atmospheric correction of CCI for the better estimate of ρ_s instead of using any constant value of τ_b in INSAT-3D AOD algorithm. After aerosol and molecular correction, ρ_s is derived for every satellite observation time. Figure 2a shows ρ_s derived from INSAT-3D ρ_{min} over the parts of Indian subcontinent countries and adjoining ocean using previous 30-day data at 0800 UTC (from 23 October to 22 November 2016) to be used for aerosol retrieval on 22 November 2016 at 0800 UTC.

Table 2
Model Parameters Varied Randomly in the Uncertainty Analysis

Random parameter	Range (minimum–maximum)
τ_b	0.01–0.15
ρ_s	0.0–0.15
$\Delta\phi$	0–180
θ_o	0–60
θ	0–60
τ	0.03–1.5
IAER	1–5
tpw	1–3

2.2.3. Retrieval of AOD

In this step precomputed LUTs are used to simulate ρ^*_{sat} for the Sun-sensor geometry and for different model AOD (τ^*) values varied from 0 to 2.5. The sensor-measured ρ_{sat} is then compared with ρ^*_{sat} by interpolation to estimate appropriate value of INSAT-3D AOD that gives the best match. The retrieval is performed only for cloud-free pixels. It is to be noted that LUTs generated using rural and maritime aerosol optical properties are used for aerosol retrieval over land and oceanic pixels, respectively. As we will see in the next section the uncertainty in aerosol retrievals increases with increasing scattering angle; therefore, aerosol retrievals with scattering angle less than 160° are only retained. Aerosol retrievals over ocean falling in glint region are also masked. Figure 2b shows the TOA apparent reflectance on 22 November 2016. The red circle shows the region with high apparent reflectance over dark water surface of the Arabian Sea due to dust transported from Iran-Pakistan region. Figure 2c shows the INSAT-3D AOD retrieval map on 22 November 2016. Figures 2d and 2e show MODIS-aqua natural color composite image and TOA INSAT-3D reflectance, respectively, where tanned dust is visible over Arabian Sea, which is clearly captured in INSAT-3D AOD map (Figure 2f).

3. Aerosol Retrieval Uncertainty Study

The uncertainty in AOD retrievals may occur due to the number of reasons such as due to uncertainties in atmospheric model, aerosol optical properties, surface reflectance variations, the RT simulation, and the uncertainty in sensor characteristics such as calibration and noise. The uncertainty in GOES-AOD (Knapp et al., 2002) was reported assuming different conditions such as low surface reflectance (<=0.12), low background aerosol conditions (<=0.04), which may not be valid for the region imaged by INSAT-3D. Moreover, the spectral response function of GOES and INSAT-3D is quite different. All these differences in atmospheric conditions, surface conditions, background aerosol conditions, and different sensor make the need of independent uncertainty analysis of the INSAT-3D AOD algorithm. The uncertainty due to RT calculation is not studied here because 6SV RT model fully takes multiple scattering into account and is able to simulate satellite-level signal within an error of 0.4–0.6% (Kotchenova & Vermote, 2007; Kotchenova et al., 2006; Vermote et al., 2006).

3.1. Uncertainty for Random Conditions

Numerous random conditions are generated for θ_o, θ, $\Delta\phi$, *IAER*, τ, τ_b, ρ_s and tpw. Here IAER stands for five aerosol models tabulated in Table 1, τ stands for AOD and other symbols are defined previously in sections 2.1 and 2.2. The range of the random variables is shown in Table 2. These are used to simulate ρ^*_{sat} and ρ_{min} using 6SV RT model, mathematically represented by

$$\rho^*_{sat} = F\left(\theta_o, \theta, \Delta\phi, \text{tpw}, \rho_s, \tau, m_i, r_{m,i}, \text{IAER}\right) \tag{4}$$

$$\rho_{min} = F\left(\theta_o, \theta, \Delta\phi, \text{tpw}, \rho_s, \tau_b, m_i, r_{m,i}, \text{IAER}\right) \tag{5}$$

here F refers to RT model function. The retrieval of surface reflectance $\rho_{r,s}$ and AOD τ_r is then performed using LUTs by adding Gaussian-distributed noise (Δ) in τ_b, m_i, r_i, ρ_{min}, ρ^*_{sat} and tpw, assuming rural aerosol model. Mathematically, the $\rho_{r,s}$ and τ_r can be represented by

$$\rho_{r,s} = F^{-1}\left(\theta_o, \theta, \Delta\phi, \text{tpw} + \Delta\text{tpw}, \rho^*_{min} + \Delta\rho^*_{min}, m_i + \Delta m_i, r_{m,i} + \Delta r_{m,i}, \tau_b + \Delta\tau_b, 1\right) \tag{6}$$

$$\tau_r = F^{-1}\left(\theta_o, \theta, \Delta\phi, \rho_{s,r}, \text{tpw} + \Delta\text{tpw}, \rho^*_{sat} + \Delta\rho^*_{sat}, m_i + \Delta m_i, r_{m,i} + \Delta r_{m,i}, 1\right) \tag{7}$$

The Gaussian distributed error Δ added to the model parameter is assumed to have zero bias, and standard deviation σ is given in Table 3. Error in retrieved τ_r and $\rho_{r,s}$ is simply given by differences

$$\rho_{e,s} = \rho_s - \rho_{r,s}; \quad \tau_e = \tau - \tau_r \tag{8}$$

The distribution of these errors is then analyzed with respect to different model parameters. Naturally, the uncertainty in τ_r and $\rho_{r,s}$ will depend on the range of model parameters used for simulating the ρ^*_{sat} and ρ_{min} which are shown in Table 2. It is to be noted that in this work the assumed maximum value of ρ_s and τ_b is set up to 0.15 and 0.15, respectively, instead of 0.12 and 0.05 which was the case studied by Knapp et al. (2002).

Table 3
The Standard Deviation σ of the Gaussian Noise Added to the Various Modal Parameters in Uncertainty Analysis for Cases A and B

Model parameter	Case A	Case B
$\sigma(\tau_b)$	0.02	0.06
$\sigma(m_{i,\ \mathrm{real}})$	0.05	0.1
$\sigma(r_i)$	20%	30%
σ(tpw)	20%	40%
$\sigma\left(\Delta\rho^*_{\mathrm{sat}}\right)$	0.004	0.004
$\sigma(\Delta\rho_{\mathrm{min}})$	0.004	0.004

The range of ρ_s and τ_b is exceeded to make conditions more representative for Indian subcontinent region. Since in tropical region the tpw acquires significantly high value, therefore, the tpw is also included as an uncertainty modal parameter both for forward modeling and for aerosol retrieval. The standard deviation of noise introduced in the model parameter for retrieval is defined for the two conditions; namely, cases A and B are shown in Table 3. The two cases are assumed such that they represent both conditions when aerosol model parameters and WV are well known (case A), while the worst case is when the assumed parameters are significantly different from the real values (case B). The lower and upper limits of the assumed uncertainty in model parameters are given as follows: $\sigma(\tau_b)$ = 0.02 and 0.06, $\sigma(m_{i,\ \mathrm{real}})$ = 0.05 and 0.1, $\sigma(r_i)$ = 20% and 30%, σ(tpw) = 20% and 40% which is equivalent to 0.4 and 0.8 cm for average condition of 2-cm WV value over Asian countries (except for monsoon season) and $\sigma\left(\Delta\rho^*_{\mathrm{sat}}\right) = \sigma(\Delta\rho_{\mathrm{min}}) = 0.004$ which is equivalent to sensor signal to noise ratio of 25 at 10% albedo. Two thousand retrievals for each case are simulated.

The summary of the retrieval uncertainty is shown in Table 4. The derived $\rho_{e,\ s}$ shows no bias with standard deviation of 0.004, while derived τ_e is biased by 0.05 and 0.11 with significant value of standard deviation equal to 0.41 and 0.66, respectively, for cases A and B. The positive biases of τ_e are due to the fact that the negative retrievals were replaced by zero value leading to positive bias. It is found that the frequency distribution of error τ_e is approximately normal; therefore, the estimated error in τ_r represented by ε_τ is calculated by finding one standard deviation of $|\tau_e|$ (i.e., the value of $|\tau_e|$ at which 68% of all $|\tau_e|$ fall below). The estimated error ε_τ equal to 0.26 and 0.37 is found in cases A and B, respectively.

To estimate the behavior of ε_τ as the function of model parameters AOD and ρ_s, the $|\tau_e|$ are arranged according to increasing values of AOD and ρ_s used in simulation. All retrievals are then divided into the finite number of bins with an equal number of entries. For each bin ε_τ is estimated and plotted with respect to modal parameters. Figures 3a and 3b show that ε_τ is strongly correlated with AOD and ρ_s for both cases A and B. Figure 3a shows an increase of 30% and 45% in ε_τ with increasing value of AOD used for simulation, for cases A and B, respectively. Figure 3c shows increasing ε_τ with increasing scattering angle Φ defined by

$$\Phi = \cos^{-1}[-\cos\theta_o\cos\theta - \sin\theta_o\sin\theta\cos\Delta\phi] \tag{9}$$

Therefore, to limit the uncertainty, INSAT-3D AOD retrievals are restricted to those pixels for which $\Phi \leq 160°$. Assuming worst retrieval conditions (case B), above analysis shows that the overall uncertainty in INSAT-3D AOD retrievals may be up to ±45% and may be less in conditions when aerosol optical properties are better known (case A).

3.2. Uncertainty of Background Aerosol

In INSAT-3D AOD algorithm, the CCI is generated by using 30-day visible data assuming that in this time window few clear-sky observations will occur without an appreciable change in ρ_s. However, in INSAT-3D view coverage area, there are several areas where even clearest possible conditions show the significant value of τ_b and high spatial as well as temporal variation in τ_b (Figure 1). For example, in winters the IG plains show elevated τ_b in range 0.15–0.2. On the other hand, some part of Asia (such as China and India) due to high traffic emissions, biomass burning, and industrialization shows significant seasonal variation in τ_b over the year. For these reasons in INSAT-3D AOD algorithm instead of using a constant value of τ_b, a dynamic climatological data set of τ_b derived from time series analysis of MODIS-aqua aerosol product has been used. However, since these climatological maps are derived from previous observations, therefore, these maps will certainly show some difference with actual τ_b. In such situation, the error in τ_b represented by $\tau_{b,\ e}$ will introduce an error in derived ρ_s leading to an uncertainty in INSAT-3D AOD. While simulating uncertainty for random conditions $\tau_{b,\ e}$ is included

Table 4
Summary of the Retrieval Uncertainty Analysis for Cases A and B, Where Conical Brackets Refer the Average of the Parameter

Parameter	Case A	Case B
$<\rho_{e,\ s}>$	0.000	0.000
$\sigma(\rho_{e,\ s})$	0.004	0.004
$<\tau_e>$	0.05	0.11
$\sigma(\tau_e)$	0.41	0.66
ε_τ	0.26	0.37

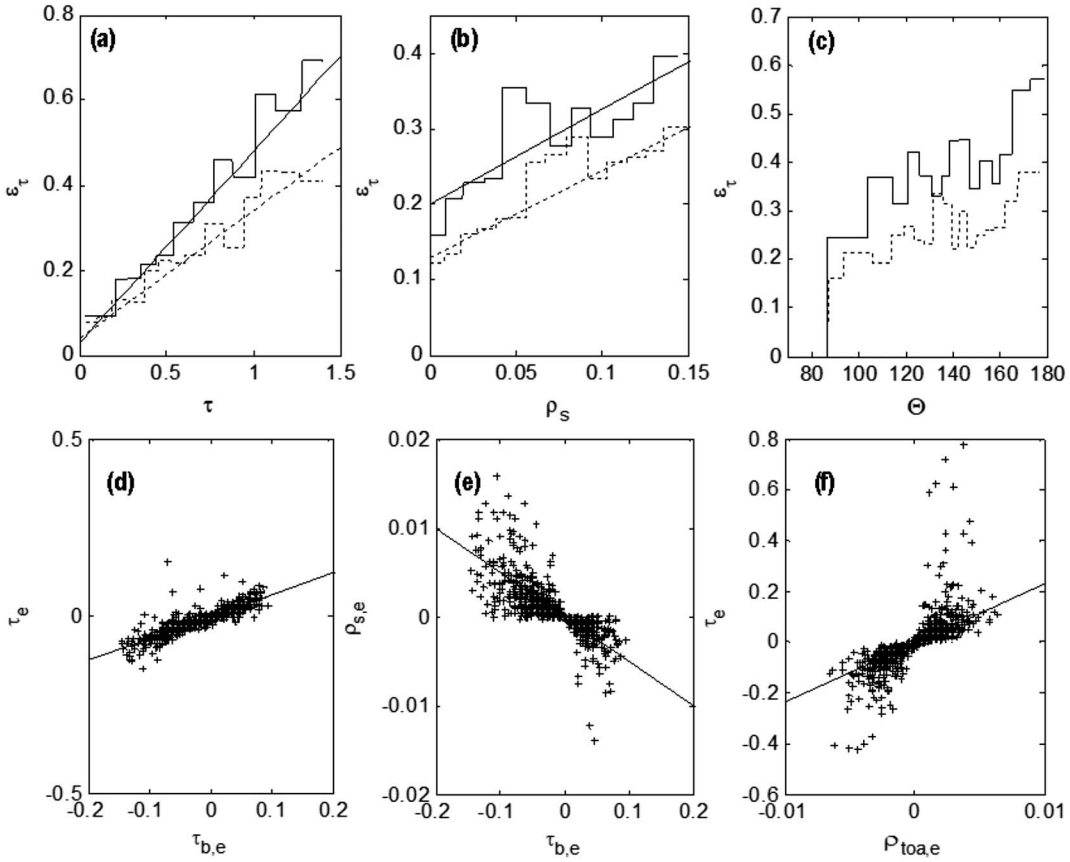

Figure 3. (a) Expected retrieval uncertainty ϵ_τ versus AOD (τ) for case A (dotted line) and case B (solid line). The linear regression is $\epsilon_\tau = 0.30\tau + 0.04$ ($r = 0.96$) for case A (dotted) and $\epsilon_\tau = 0.45\tau + 0.03$ ($r = 0.97$) for case B (solid). (b) Expected retrieval uncertainty ϵ_τ versus ρ_s for case A (dotted line) and case B (solid line). The linear regression is $\epsilon_\tau = 1.164\rho_s + 0.13$ ($r = 0.89$) for case A (dotted) and $\epsilon_\tau = 1.27\rho_s + 0.20$ ($r = 0.81$) for case B (solid). (c) Expected retrieval uncertainty ϵ_τ versus scattering angle Φ for case A (dotted) and case B (solid). (d) Error in aerosol optical depth τ_e versus error in background aerosol optical depth $\tau_{b,\,e}$. The linear regression is $\tau_e = 0.62\tau_{b,\,e} - 0.001$ ($r = 0.88$). (e) Error in surface reflectance $\rho_{s,\,e}$ versus error in background aerosol optical depth $\tau_{b,\,e}$. The linear regression is $\rho_{s,\,e} = -0.05\tau_{b,\,e} + 0.0001$ ($r = 0.70$). (f) Error in aerosol optical depth τ_e versus error in top-of-atmosphere satellite measurement $\rho_{\mathrm{toa},\,e}$. The linear regression is $\tau_e = 23.27\rho_{\mathrm{toa},\,e} - 0.003$ ($r = 0.86$).

but to understand properly the effect of $\tau_{b,\,e}$ explicitly on AOD retrievals, a separate 2,000 simulations of retrieval errors $\rho_{s,\,e}$ and τ_e assuming random Gaussian error in τ_b with standard deviation of 0.06 are performed and results are plotted in Figures 3d and 3e as a function of $\tau_{b,\,e}$. For simulation, zenith and azimuth angles used are similar to that given in Table 2. It is clear that if τ_b is underestimated, less aerosol scattering from the CCI will be corrected leading to an overestimated value of ρ_s resulting in an underestimated AOD. The linear regression slope is 0.624 with a strong correlation coefficient of 0.88 which suggests retrieval uncertainty of $\tau_e = 0.624\tau_{b,\,e}$. Therefore, error in τ_b gets transformed to an error in AOD but is not amplified with AOD, instead strongly depends on the value of τ_b. Since climatological data set of τ_b has been used in the INSAT-3D AOD algorithm, $\tau_{b,\,e}$ is not expected to exceed by 0.15, which is equivalent to a maximum error of 0.09 in AOD.

3.3. Uncertainty of Satellite Measurement

Satellite measurement errors although included in uncertainty for the random condition, a separate simulation for uncertainty in retrieved AOD as a function of the error in satellite measurement is done and the results are shown in Figure 3f. The error in TOA satellite measurement, that is, $\rho_{\mathrm{toa},e} = \Delta\rho^*_{\mathrm{sat}}$ is varied from -0.008 to 0.008 with 2,000 random Sun-sensor geometries and molecular plus aerosol-mixed atmosphere with optical depth range described in Table 2. These errors give lowest signal-to-noise ratio of 18.0 at 15% albedo which is less than the signal-to-noise ratio of INSAT-3D when binned at 10-km spatial resolution. The simulated results of τ_e as a function of $\rho_{\mathrm{toa},\,e}$ are shown in Figure 3f. The linear regression slope is

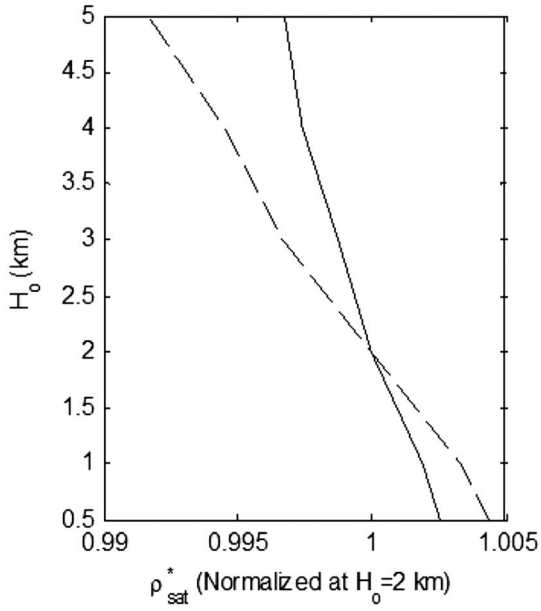

Figure 4. Top-of-atmosphere simulated reflectance ρ^*_{sat} normalized at an aerosol scale height H_o = 2 km versus H_o for AOD = 0.5 (solid line) and AOD = 1.0 (dashed line) assuming rural aerosol model. AOD = aerosol optical depth.

23.27 with a strong correlation coefficient of 0.86 which suggests retrieval uncertainty of $\tau_e = 23.27\rho_{toa,\ e}$. Therefore, for INSAT-3D AOD retrievals $\tau_e < 0.18$ is expected.

3.4. Uncertainty of Aerosol Profile

In INSAT-3D AOD algorithm the retrieval is achieved by using LUTs which are generated assuming an exponential aerosol profile with the scaled height H_o of 2 km. However, from different reports (Hayasaka et al., 2007; Winker et al., 2013) it is found that H_o of the aerosol vertical profile may vary in a range of 0.5 (in winters) to 5 km (summers). To simulate this uncertainty, ρ^*_{sat} are modeled assuming different values of H_o. The ratio defined as ρ^*_{sat} at different H_o normalized by ρ^*_{sat} at H_o = 2 km for the two cases, moderately thin aerosol layer (AOD = 0.5), and thick aerosol layer (AOD = 1.0) for H_o = 0.5 to 5 km is shown in Figure 4. The assumed aerosol model is rural, and geometry is selected such that scattering angle $\Phi \leq 160°$, which corresponds to poorest retrieval conditions (see Figure 3c, $\varepsilon_\tau$versus Φ). From Figure 4 it is clear that when the aerosol layer is thin no significant change in ratio is observed (~1.0), while for thick aerosol layer the maximum change is 0.99 equivalent to an error of 0.002 in $\rho^*_{sat} = 0.2$ at H_o = 2 km which corresponds to τ_e = 0.05. Winker et al. (2013), using CALIOP data found that in INSAT-3D view coverage the change in H_o ranges from 0.5 to 3 km over the year; therefore, uncertainty in INSAT-3D AOD due to the error in H_o must not exceed by 0.05.

3.5. Other Sources of Uncertainty

In this section other sources of uncertainty are discussed which are either not possible to model or are not sensor specific; therefore, study for GOES-AOD presented in Knapp et al. (2002) is valid for INSAT-3D AOD too. The nonspherical shapes of aerosol particle may also introduce some error in τ retrievals; however, error due to spherical shape assumption is high only for large-sized particles such as desert dust, whereas optical properties of rural aerosol model which are dominated by small-sized particles can be well represented by assuming spherical shape (Li et al., 2013; Martins et al., 1998). Therefore, little uncertainty due to spherical shape assumption is likely to be introduced in INSAT-3D AOD retrievals. Ignoring the effect of bidirectional reflectance distribution function (BRDF) of surface while retrieval is expected to introduce uncertainty of less than 15% (Knapp et al., 2002) due to the fact that geostationary platforms provided static view geometry and less variation in solar geometry at a given time of the day over a time period of 30 days. The uncertainty due to surface variation (due to the seasonal growth cycle of vegetation or due to rainfall) is also expected to be small since only 30-day time window has been used for determining the CCI. The uncertainty due to the error in simulation of the gaseous absorption (error in tpw) has already been included while simulating the random condition (section 3.1).

3.6. Overall Uncertainty

From the linear regression results shown in Figure 3, it is evident that the retrieval uncertainty in INSAT-3D AOD may fall in the range of 30% to 45% over land depending on the uncertainty of the aerosol optical properties used in retrieval algorithm, the instrument measurement error, the background AOD, and the gaseous absorption. However, there may be less likely conditions such as very bright surface ($\rho_s > 0.15$), presence of dust particles (nonspherical particles), aerosol vertical profile with very high aerosol scale height, significant BRDF effect, and strong variation of surface reflectance within 30-day time window in which retrieval uncertainty may rise beyond the limit of 45%. Overall, the retrieval uncertainty will be less than 45% in most of the conditions representative of the INSAT-3D view coverage area over land.

The results presented in Figures 3 and 4 are valid for land surface. Similar analysis for INSAT-3D AOD retrieval over ocean has been done where the maritime aerosols are used for simulating ρ^*_{sat} and ρ_{min} as well as for AOD retrieval. While AOD retrieval the added Gaussian-distributed errors and the range of model parameters used are similar to the case of land described in Tables 3 and 2, respectively, except for surface reflectance.

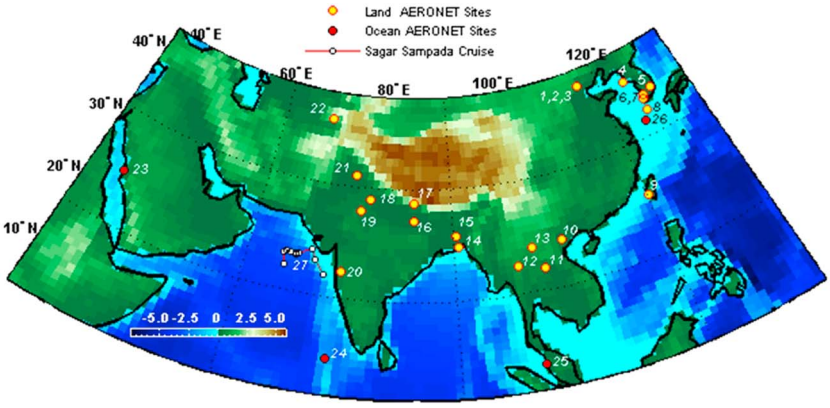

Figure 5. Map showing the location of land AERONET stations (1 to 22), ocean AERONET stations (23–26), and Sagar Sampada station points (27) as tabulated in Table 5. AERONET = Aerosol Robotic Network.

The range of surface reflectance assumed for ocean surface is 0.0 to 0.015. An uncertainty of $<$30% is found for AOD retrievals over oceans.

4. INSAT-3D Retrieval Validation

4.1. Validation With the Ground Truth

The ground observation of AOD by AERONET, $\tau_{AERONET}$ at various locations, and by handheld Sun-photometer during the Sagar Sampada (SS-348) cruise, τ_{SS-348} are used for the validation of INSAT-3D AOD retrievals, $\tau_{INSAT-3D}$. AERONET is a worldwide network of the ground-based Sun-sky radiometer, which provides excellent measurements of AOD with low uncertainty (±0.02) and high temporal resolution of about 15 min on average (Holben et al., 1998). In this work, 26 AERONET stations falling in the vicinity of INSAT-3D view coverage are selected, out of which 22 represent inland observation, while 4 of these represent the oceanic observations. Only those stations are assumed to be oceanic for which the nearest pixel in INSAT-3D AOD product shows elevation $\leq$0. The location of all ground stations and the path of SS-348 cruise are shown in Figure 5.

The station number, name, location, country, and general remarks on the type of the station are tabulated in Table 5. The general remarks given in Table 5 are based on information given at AERONET website for each site (https://aeronet.gsfc.nasa.gov/). Neither the AERONET station nor the handheld Sun photometer provides AOD at 0.55 μm, while $\tau_{INSAT-3D}$ is derived at 0.55 μm; therefore, second-order polynomial interpolation of spectral $\tau_{AERONET}$ is performed to derive $\tau_{AERONET}$ at 0.55 μm. AERONET observation shows very low uncertainty in their measurement; however, due to spatial inhomogeneity of AOD, there will be significant uncertainty when comparing with $\tau_{INSAT-3D}$, because INSAT-3D observations are at coarser spatial resolution while AERONET being point observation measures only a fraction of aerosols sampled by INSAT-3D. The spatial inhomogeneity is mainly introduced due to dynamic motion of atmosphere and different aerosol sources near the AERONET sites (Ichoku et al., 2002). For this reason, following the spatiotemporal approach described by Ichoku et al. (2002), the temporal average of $\tau_{AERONET}$ in a time window of ±30 min is used for comparison with $\tau_{INSAT-3D}$ averaged over a spatial window of 5 × 5 pixels, that is, 50 × 50 km^2 area. Only those data points were considered in which at least 3 $\tau_{AERONET}$ and 12 $\tau_{INSAT-3D}$ valid observations exist in ±30-min time window and 5 × 5 pixels spatial widow, respectively. In general, the spatial variation of aerosols is smoother; however, the cloud contamination introduces noise in retrieved AOD; therefore, standard deviation test can be used to reject the AOD pixels that might potentially have contaminated by cloud edges or residual subpixel clouds (Kolmonen et al., 2013; Prados et al., 2007). In present work, the data points with the standard deviation of $\tau_{INSAT-3D}$ in 5 × 5 pixels spatial widow greater than 0.2 are rejected to decrease the effect of cloud contamination in the validation study. The threshold value of 0.2 used here is near to the globally excepted threshold for filtering the cloud-contaminated AOD retrievals (Kolmonen et al., 2013; Prados et al., 2007). One more point to be noted is that cloud-screened L1.5 AERONET data are used for validation due to the unavailability of L2 data for the whole year of 2016 at all locations.

Table 5
Information About the AERONET Stations Used in INSAT-3D AOD Validation

Station no.	Station name	Longitude(°E)/latitude(°N)	Country	Remarks
1	Beijing-CAMS	116.32/39.93	China	Urban, traffic, and industrial pollution
2	Beijing	116.38/39.97	China	Urban, traffic, and industrial pollution
3	Beijing-PKU	116.31/39.91	China	Urban, traffic, and industrial pollution
4	Baengnyeong	124.63/ 37.96	South Korea	Coastal, forest, and no pollution sources
5	KORUS_Kyungpook	128.61/35.89	South Korea	Urban
6	Gwangju_GIST	126.84/35.23	South Korea	Semiurban, outskirt of Gwangju city, and transported pollution
7	KORUS_Mokpo_NU	126.44/34.91	South Korea	Urban
8	Gosan_SNU	126.16/33.29	Je-ju Island, South Korea	Vegetated and no source of artificial pollution
9	Chen_Kung_University	98.97/18.77	Taiwan	Urban, polluted, and near railway station
10	NGHIA_DO	105.80/21.05	Vietnam	Urban and polluted
11	Nong_Khai	102.72/17.88	Thailand	Rural, biomass burning, and agriculture activity
12	Chiang_Mai_Met_Sta	98.97/18.77	Thailand	Urban, polluted, and near Chiang Mai airport
13	Luang_Namtha	101.42/20.93	Thailand	Rural and agriculture activity
14	Bhola	90.75/22.17	Bangladesh	Rural, biomass burning, and agriculture activity
15	Dhaka University	90.40/23.73	Bangladesh	Traffic and industrial pollution
16	Ghandhi_College	84.13/25.87	India	Rural, biomass burning, and transported pollution
17	Pokhara	83.97/28.15	Nepal	Rural/mountainous
18	Gual_Pahari	77.15/28.43	India	Urban, traffic, and industrial pollution
19	Jaipur	75.81/26.91	India	Semiarid, traffic emission, and dust transport
20	Pune	73.85/18.53	India	Urban and heavy traffic emission
21	Lahore	74.32/31.54	Pakistan	Semiarid/urban, heavy traffic, and industrial pollution
22	Dushanbe	68.86/38.55	Tajikistan	Urban, traffic, and industrial pollution
23	KAUST_Campus	39.01/22.30	Saudi Arabia	Red sea, just at sea shore, and marine aerosols
24	MCO-Hanimaadhoo	73.18/6.78	Maldives	Indian ocean, no local pollution, and mostly marine aerosols
25	USM_Penang	100.302/5.36	Malaysia	South China Sea, 2 km away from sea, mostly marine aerosols, and transported industrial pollution also
26	Ieodo_Station	125.18/32.12	South Korea	East China Sea and marine aerosol
27	Sagar Sampada (SS-348) Cruise	Path shown in Figure 5		North Arabian Sea and marine aerosol

4.1.1. Validation Results Over Ocean

The validation of INSAT-3D AOD with ground observations for oceanic sites 23-27 is plotted in Figure 6. The linear regressions statistics of these validations are provided in Table 6. High correlation coefficients, *r*, are found at all four oceanic AERONET sites and one SS-348 cruise, with *r* ranging from 0.79 to 0.91. Slopes of the linear regression lines show variation about 1% by 22%, probably caused by spatial variations in the aerosol optical properties. The small bias at site numbers 23, 24, 25, and 27 is within the expected noise and may be due to the assumption of ignorance of BRDF effect caused by winds over the ocean surface. The significant negative bias of −0.09 at Ieodo-station (site 26) may be due to the low viewing angle which makes INSAT-3D

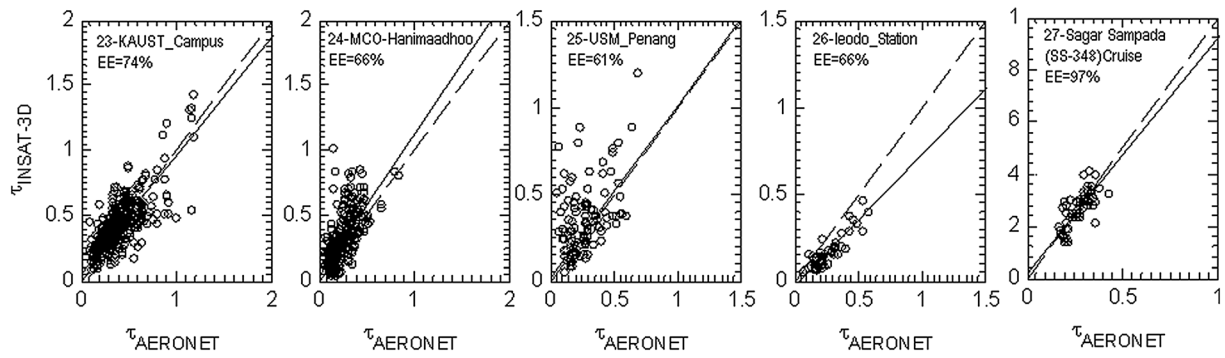

Figure 6. INSAT-3D versus AERONET aerosol retrieval in 2016 over oceanic stations. EE stands for number of data points falling within the expected error envelope. INSAT-3D = Indian National Satellite; AERONET = Aerosol Robotic Network.

Table 6
The Linear Regressions Statistics for the Validation of INSAT-3D AOD and AERONET-AOD Retrievals Over Four Oceanic AERONET stations and SS-348 cruise Points Including the Number of Data Points N, Correlation Coefficient r, Linear Regression Slope m, Linear Regression Offset i, Root Mean Square Error σ_τ, Bias, Mean AERONET-AOD $\langle\tau_{\text{aeronet}}\rangle$, Mean INSAT-AOD $\langle\tau_{\text{INSAT}}\rangle$, and Relative Error $\sigma_\tau/\langle\tau_{\text{aeronet}}\rangle$)

Station no.	*N*	*m*	*i*	*r*	σ_τ	Bias	$\langle\tau_{\text{aeronet}}\rangle$	$\langle\tau_{\text{INSAT}}\rangle$	$\sigma_\tau/\langle\tau_{\text{aeronet}}\rangle$
23	298	0.91	0.050	0.84	0.1	−0.003	0.40	0.40	0.25
24	324	1.09	0.030	0.81	0.08	0.05	0.27	0.33	0.30
25	95	0.99	0.020	0.79	0.1	0.04	0.29	0.35	0.34
26	63	0.78	−0.030	0.91	0.03	−0.09	0.22	0.15	0.14
27	64	0.91	0.015	0.81	0.03	−0.007	0.27	0.26	0.11

Note. INSAT-3D = Indian National Satellite; AOD = aerosol optical depth; AERONET = Aerosol Robotic Network.

looking different aerosol column relative to the AERONET observation. Except for site 25, the relative error of estimates ($\sigma_\tau/\langle\tau_{\text{aeronet}}\rangle$), that is, the standard error of regression (σ_τ) compared to the average observed optical depth ($\langle\tau_{\text{aeronet}}\rangle$) ranges from 0.11 to 0.30. The larger relative errors of 0.34 for site 25 (USM_Penang) located ~2-km inland from the shoreline of South China Sea may be associated with transported industrial pollution from Penang city and lower $\langle\tau_{\text{aeronet}}\rangle$. The validation herein shows results within the ±30% range.

4.1.2. Validation Results Over Land

The validation for land sites 1–22 is plotted in Figure 7, and the linear regressions statistics of these validations are provided in Table 7. Excluding sites 10, 16, 18, and 21, discussed later, high correlation coefficients, *r*, are found at rest 18 AERONET sites, with *r* ranging from 0.70 to 0.91. Slopes of the linear regression lines show significant variation about 1% by 39%, probably caused by large spatial variations in the aerosol optical properties. At majority of land sites, negative bias in retrieved $\tau_{\text{INSAT}-3\text{D}}$ ranging between −0.25 and −0.03 is observed. The relative error of estimates ($\sigma_\tau/\langle\tau_{\text{aeronet}}\rangle$) for these 18 sites ranges from 0.19 to 0.46. The large deviation in the slope of linear regression equal to 0.37 to 0.59 with small correlation coefficients, *r*, equal to 0.74 and 0.50 over sites 16 and 18 is not only due to the difference in assumed aerosol optical properties but also probably due to the dominance of fine mode aerosols from biomass burning and low planetary boundary layer over Indian region during the winter season. The AERONET sites 16 and 18 are situated in IG plain where the planetary boundary layer decreases up to 0.5 km in winters with heavy biomass burning, while in summers transported dust from western India and other western countries makes retrieval assumption such as 2-km scaled height of aerosol vertical profile and static rural aerosol model invalid, resulting to the underestimation of $\tau_{\text{INSAT}-3\text{D}}$. The lower slope and correlation coefficient equal to 0.51 and 0.55, respectively, for Lahore (site 21) is observed. The Lahore is a semiarid and heavily polluted urban area due to traffic and industrialization. The traffic and industrial pollution led to absorbing and fine mode aerosol particles with optical properties significantly different than those of rural aerosols. Similar reasons may explain the significant deviation of linear regression slope (47%) from unity and lower correlation coefficient ($r = 0.65$) for site 10. The large intercept of linear regression line ranging from 0.15 and 0.32 is due to the substantial uncertainty in surface reflectance determination over these four sites. All four sites especially Indian sites 16 and 18 suffer from persistent heavy pollution over the year, and therefore, less probability of getting enough cloud-free clean conditions in terms of low aerosol loading is generally obtained leading to large uncertainty in surface reflectance and $\tau_{\text{INSAT}-3\text{D}}$. The validation herein shows results within the range of 45% uncertainty.

4.1.3. Overall Validation With Ground Truth

To estimate overall performance of $\tau_{\text{INSAT}-3\text{D}}$ over land and ocean, all available data points are compared with ground truth data. The validation of $\tau_{\text{INSAT}-3\text{D}}$ over oceanic and land site is shown in Figures 8a and 8b, respectively. For the case of land, the data points corresponding to site 10, 16, 18, and 21 are excluded while doing regression analysis. In totality extensive validation of $\tau_{\text{INSAT}-3\text{D}}$ with ground truth is plotted in Figures 8a and 8b that encompasses a total of 855 and 3,133 collocated data points in space and time for ocean and land sites, respectively. The slope of regression line for the ocean is 0.87 which is 13% off from the unity, while a strong correlation coefficient of 0.77 is found. Similarly, for land sites the slope and correlation coefficient of 0.61 and 0.69, respectively, are observed. The lower value of correlation coefficient over land is due to the scattered outliers; to avoid this and for getting more clear overall validation statistics, all 855 and 3,133 data points for ocean and land sites are divided into 16 and 42 bins each

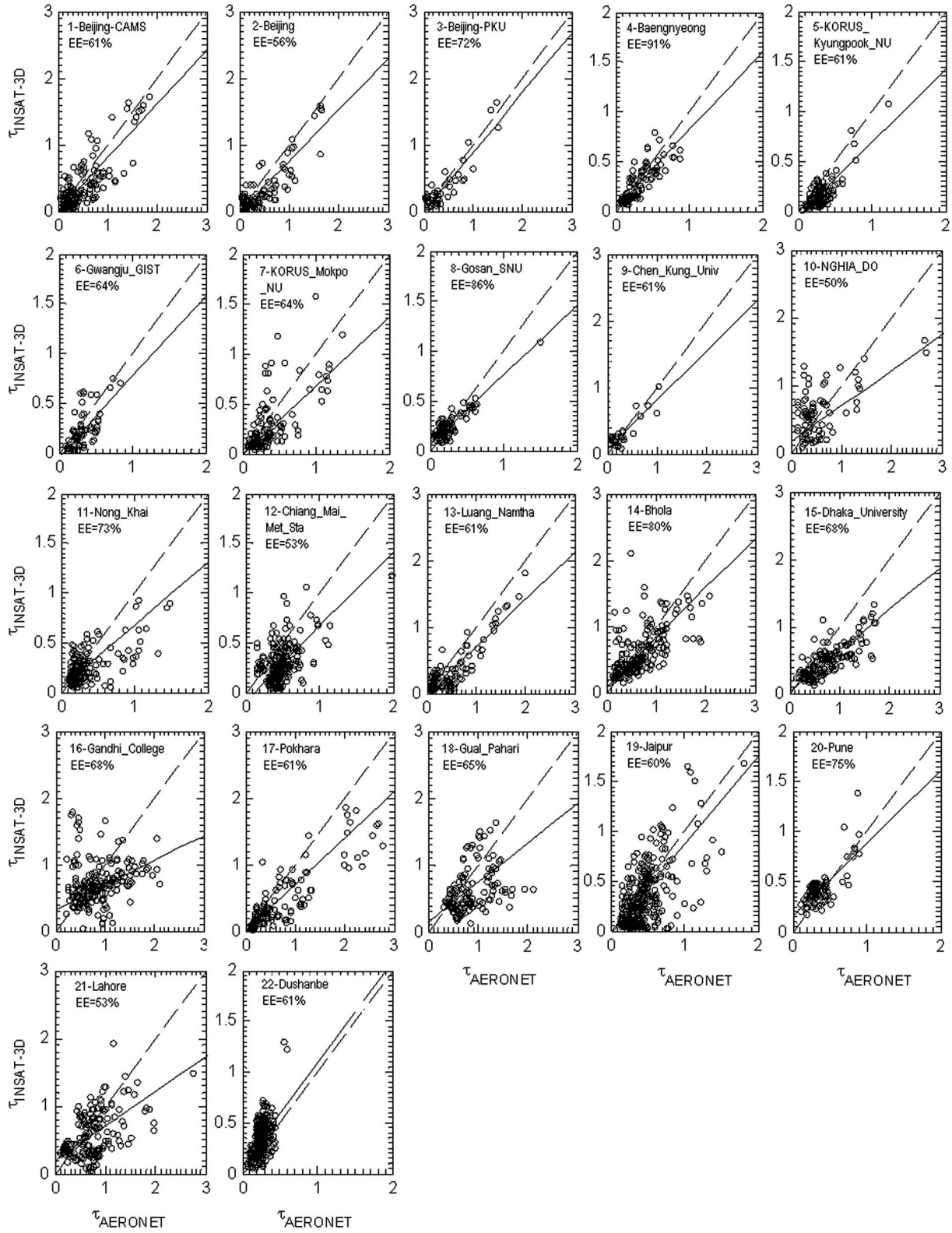

Figure 7. Scatter plot between INSAT-3D and AERONET aerosol retrieval in 2016 over land stations. EE stands for number of data points in percent falling within the expected error envelope. INSAT-3D = Indian National Satellite; AERONET = Aerosol Robotic Network.

Table 7
Same as Table 6 but Here for 22 Land Stations

Station no.	N	m	i	r	σ_τ	Bias	$\langle\tau_{aeronet}\rangle$	$\langle\tau_{INSAT}\rangle$	$\sigma_\tau/\langle\tau_{aeronet}\rangle$
1	211	0.81	−0.007	0.83	0.18	−0.08	0.45	0.38	0.40
2	116	0.77	−0.02	0.87	0.12	−0.10	0.40	0.32	0.30
3	56	0.89	−0.002	0.91	0.14	−0.06	0.39	0.33	0.36
4	156	0.79	0.027	0.86	0.08	−0.03	0.26	0.23	0.31
5	166	0.74	−0.050	0.76	0.08	−0.13	0.30	0.18	0.27
6	80	0.81	−0.035	0.74	0.11	−0.09	0.31	0.24	0.35
7	245	0.69	−0.009	0.90	0.09	−0.10	0.34	0.25	0.26
8	125	0.70	0.060	0.86	0.06	−0.01	0.25	0.24	0.24
9	39	0.74	0.070	0.81	0.14	0.03	0.30	0.34	0.46
10	87	0.53	0.160	0.65	0.25	−0.01	0.54	0.54	0.46
11	226	0.63	0.050	0.83	0.09	−0.06	0.31	0.25	0.29
12	226	0.75	−0.080	0.71	0.15	−0.16	0.48	0.31	0.31
13	123	0.71	−0.010	0.87	0.15	−0.09	0.46	0.36	0.33
14	214	0.75	0.080	0.83	0.15	−0.08	0.65	0.57	0.23
15	213	0.61	0.040	0.84	0.14	−0.22	0.73	0.54	0.19
16	255	0.37	0.320	0.74	0.19	−0.12	0.85	0.73	0.22
17	214	0.71	−0.020	0.87	0.15	−0.15	0.43	0.33	0.35
18	149	0.59	0.150	0.50	0.29	−0.22	0.80	0.62	0.36
19	345	0.89	−0.030	0.70	0.20	−0.10	0.45	0.36	0.44
20	105	0.73	0.150	0.71	0.12	0.07	0.35	0.40	0.34
21	179	0.51	0.200	0.55	0.21	0.001	0.61	0.61	0.34
22	273	1.01	0.080	0.70	0.12	0.10	0.28	0.38	0.42

carrying approximately 53 and 74 points, respectively. The mean value of $\tau_{INSAT-3D}$ and ground truth in each bin is then plotted and shown in Figures 8c and 8d. Both over land and ocean strong correlation coefficient $>$ 0.9 is observed. The slope of regression line for the ocean is equal to 0.91, while for land no significant improvement is observed. The improvement in correlation coefficient is because binning of $\tau_{INSAT-3D}$ in the finite number of bins decreases the effect of outliers. The improvement in slope over ocean site is because of less contribution from the small number of data points from site 26 which independently show low slope and low $\langle\tau_{INSAT}\rangle$. In summary, the validation outcomes show the overall uncertainty of less than 30% and 45% over ocean and land, respectively, which is in agreement with theoretical uncertainty analysis in section 3. The better performance of INSAT-3D AOD algorithm over ocean relative to land is due to the fact that ocean surface is almost dark (derived surface reflectance mostly less than 0.015) and less heterogeneous than land surface. Moreover, aerosol optical properties of aerosol over the ocean are less diverse than that over land leading to less uncertainty in derived $\tau_{INSAT-3D}$ over ocean.

4.2. Comparison With the Monthly Mean of MODIS Retrieval

To explore the possibility of using combined polar satellite and INSAT-3D AOD for the climatological study of Earth, the comparison of MODIS-aqua and the INSAT-3D derived AOD is done over Indian landmass, Arabian Sea, and BOB. The monthly mean of the dark target and deep blue combined MODIS-aqua AOD (τ_{MODIS}) downloaded from Giovanni portal at 1 × 1° resolution is used (https://giovanni.gsfc.gov/). Since MODIS-aqua pass time over Indian landmass, Northeast Arabian Sea and BOB roughly range from 0700 to 0830 UTC; therefore, the temporal monthly average of all τ_{INSAT} derived between times 0700 and 0830 UTC is generated. The 10-km INSAT-3D monthly means are then spatially averaged at 1 × 1° grid collocated with MODIS monthly mean grid. It is worth mentioning that while doing average only glint-free and cloud-free τ_{INSAT} are used. Only those locations are used for comparison where at least 12 (approximately 40% of the days in a month) valid daily average observations of τ_{INSAT} at a given location in a month are found. No data during months of May to August are obtained over oceanic region of interest due to significant cloud cover and Sun glint; therefore, these months are excluded from the comparison. Whereas, over Indian landmass, during months of July and August falling in the middle of monsoon season almost no valid data are available due to heavy cloud cover; therefore, over land these 2 months are excluded while doing the comparison.

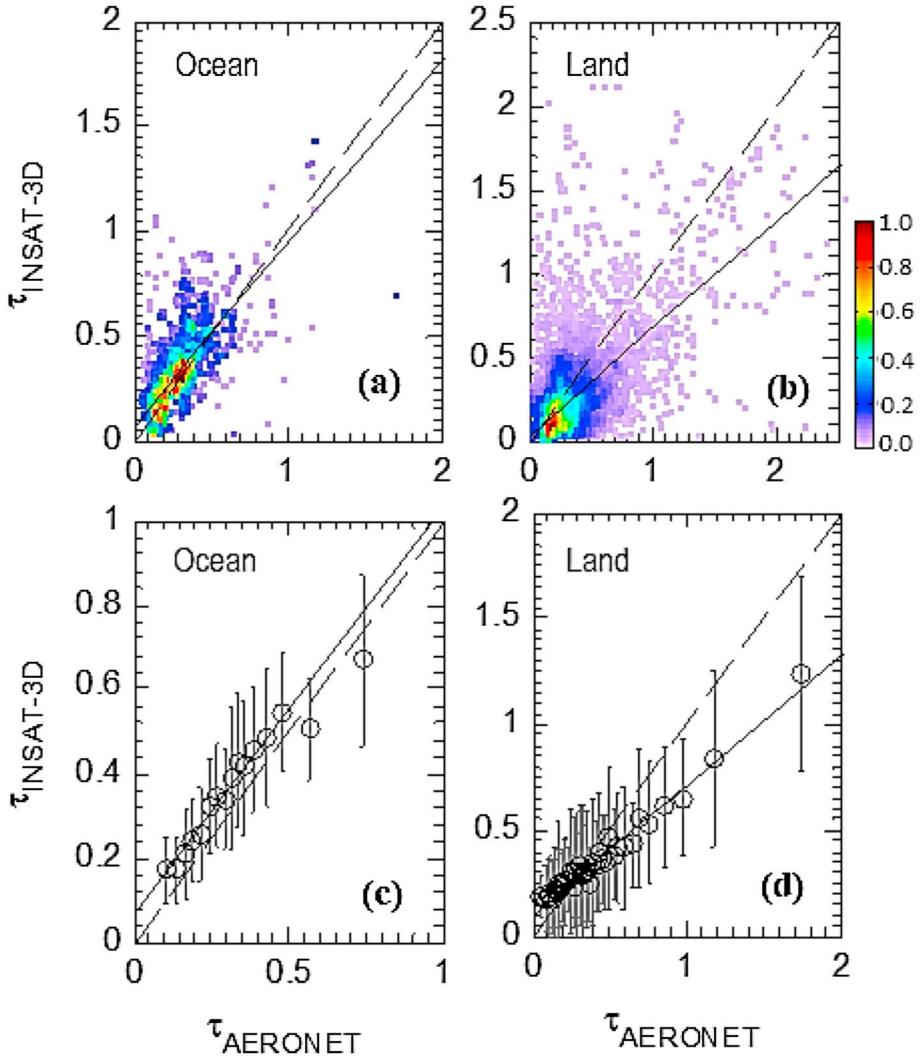

Figure 8. (a) and (b) Scatter plot of INSAT-3D and AERONET AOD for all sites over ocean and land sites, respectively. For the case of land (Figure 8b) the site with numbers 10, 16, 18, and 21 is excluded. For land, the linear regression is $\tau_{INSAT-3D} = 0.61\tau_{AERONET} + 0.07$ ($r = 0.69, \sigma_\tau = 0.15$, bias = $-0.07, \sigma_\tau/\langle\tau_{aeronet}\rangle = 0.36$), while for ocean the linear regression is $\tau_{INSAT-3D} = 0.87\tau_{AERONET} + 0.08$ ($r = 0.77, \sigma_\tau = 0.10$, bias = $0.05, \sigma_\tau/\langle\tau_{aeronet}\rangle = 0.29$) . (c) and (d) The scatter between the binned INSAT-3D and in situ AOD over all land and ocean sites, respectively. For land (ocean) sites all AERONET AODs were sorted and divided into 42 (16) bins with almost 74 (53) data points in each bin. The average values are represented by scatter bubbles, and vertical lines show standard deviation of INSAT-3D AOD in each bin. For land the linear regression is $\tau_{INSAT-3D} = 0.61\tau_{AERONET} + 0.09$ ($r = 0.91, \sigma_\tau = 0.06$) . For ocean the linear regression is $\tau_{INSAT-3D} = 0.96\tau_{AERONET} + 0.07$ ($r = 0.89, \sigma_\tau = 0.05$) . Bining of INSAT-3D AOD significantly decreases the noise, and therefore, high correlation is obtained.

4.2.1. Comparison Results Over the Ocean

The comparison between monthly averaged MODIS-AOD and INSAT-3D AOD for Arabian Sea and BOB is plotted in Figure 9. The linear regression statistics of these comparisons are provided in Table 8. Excluding October, high correlation coefficients, *r*, are found in all months, with *r* ranging from 0.72 to 0.97. The moderate value of correlation coefficient equal to 0.65 during October is probably associated with uncertainty in optical properties over Arabian Sea due to dust contamination. The transition of weather pattern over the Arabian Sea occurs during October. During the summers the winds blow from the sea toward land, while in the winter, winds blow over the Arabian Sea from the northeast. During October falling between the summer and winter monsoons, the existing wind direction varies due to which dust transportation from land to Arabian Sea takes place. During 25–27 October 2016, due to strong northeasterly winds, several dust plumes off the coast of Iran and Pakistan were observed by Visible Infrared Imaging Radiometer Suite on Suomi NPP (https://earthobservatory.nasa.gov/NaturalHazards/view.php?id=89013). The contamination of dust significantly changed the optical properties of aerosol over Arabian Sea, while in INSAT-3D AOD fixed maritime

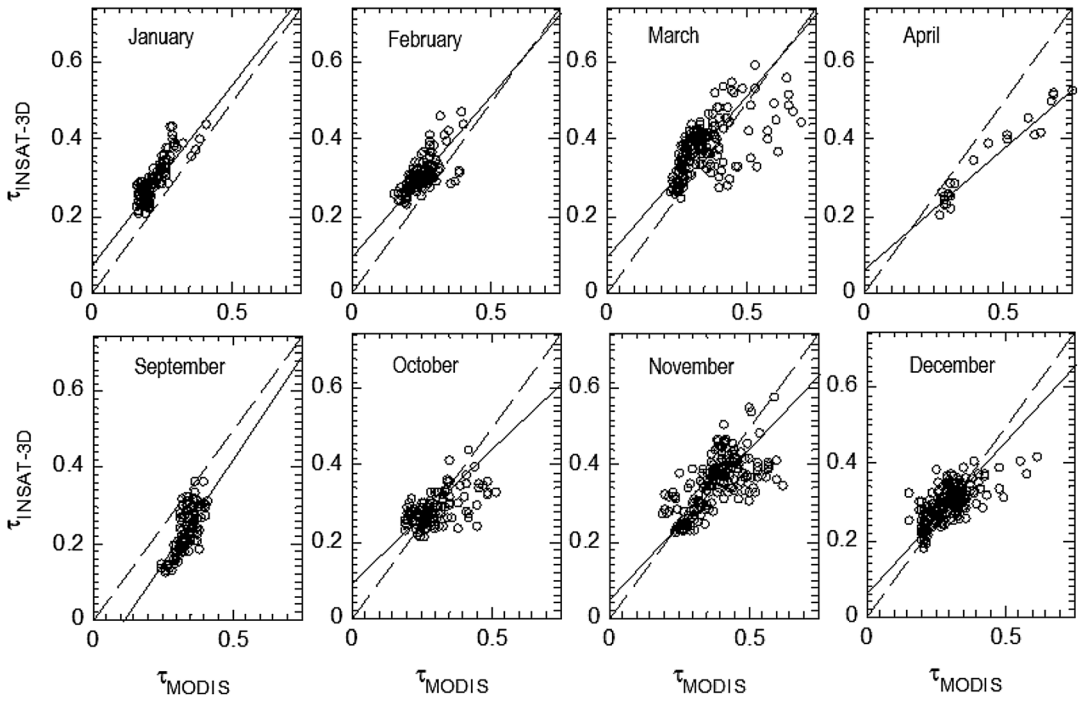

Figure 9. Scatter plot between monthly average INSAT-3D and MODIS AOD retrievals over Arabian Sea and Bay of Bengal region at 1° resolution at around 730–800 UTC. May to August plots are not shown due to very less number of cloud- and glint-free retrievals. INSAT-3D = Indian National Satellite; MODIS = Moderate Resolution Imaging Spectroradiometer; AOD = aerosol optical depth.

aerosol model is used leading to the low correlation coefficient. Slopes of the linear regression lines show variation about 1% by 30%, probably caused by uncertainty in the aerosol optical properties due to the temporal and spatial variation of relative humidity. The significant bias in April may be due to the assumption of ignorance of BRDF effect caused by strong winds over the ocean surface and very less number of data points. The spatial and temporal averaging of INSAT-3D AOD retrievals at 1 × 1° resolution grid significantly decreases the noise resulting to small relative error of estimates ($\sigma_\tau/\langle\tau_{\text{aeronet}}\rangle$) ranging from 0.05 to 0.14. The comparison results over Arabian Sea and BOB show overall error of 14% in INSAT-3D AOD relative to MODIS-AOD.

4.2.2. Comparison Results Over Land

The comparison between monthly averaged MODIS-AOD and INSAT-3D AOD over Indian landmass is plotted in Figure 10. The linear regressions statistics of these comparisons are provided in Table 9. Excluding the dusty season March and April, high correlation coefficients, *r*, are found in all months, with *r* ranging from 0.74 to 0.89. The relative error of estimates ranges from 0.15 to 0.27. The small value of correlation coefficient equal to 0.52 and 0.45 and large relative error of estimates 0.31 and 0.76 during March and April, respectively,

Table 8
Same as Table 7 but Here Validation With Monthly Mean MODIS-Aqua AOD Over Arabian Sea and Bay of Bengal Region at 1° Resolution

Month	*N*	*m*	*i*	*r*	σ_τ	Bias	$\langle\tau_{\text{MODIS}}\rangle$	$\langle\tau_{\text{INSAT}}\rangle$	$\sigma_\tau/\langle\tau_{\text{MODIS}}\rangle$
January	138	0.94	0.07	0.84	0.03	0.06	0.22	0.28	0.13
February	138	0.85	0.09	0.81	0.03	0.05	0.26	0.30	0.12
March	151	0.85	0.09	0.81	0.04	0.03	0.35	0.38	0.11
April	26	0.70	0.03	0.97	0.03	−0.14	0.59	0.45	0.05
September	104	1.15	−0.15	0.72	0.04	−0.09	0.33	0.23	0.12
October	131	0.70	0.08	0.65	0.03	−0.01	0.30	0.29	0.10
November	192	0.78	0.06	0.76	0.05	−0.03	0.38	0.35	0.13
December	195	0.80	0.06	0.74	0.03	0.0	0.30	0.30	0.10

Note. MODIS = Moderate Resolution Imaging Spectroradiometer; AOD = aerosol optical depth.

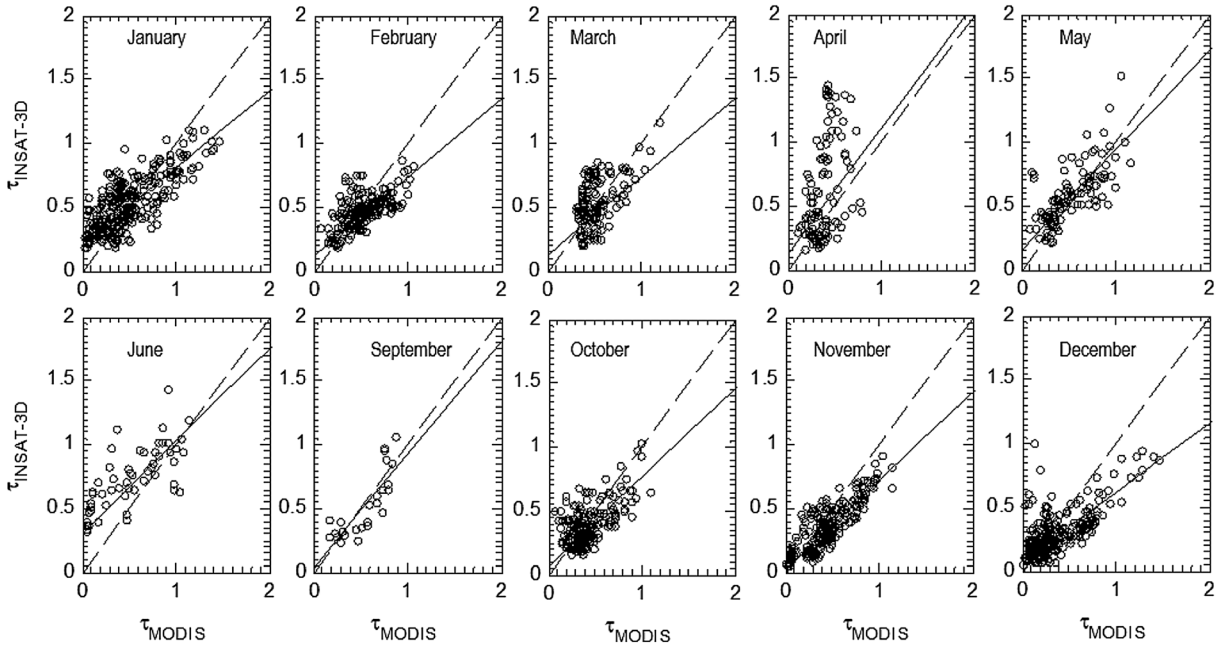

Figure 10. Scatter plot between monthly average INSAT-3D and MODIS AOD retrievals over Indian and neighboring country landmass region at 1° resolution at around 730–800 UTC. July and August plots are not shown due to very less cloud-free pixels. INSAT-3D = Indian National Satellite; MODIS = Moderate Resolution Imaging Spectroradiometer; AOD = aerosol optical depth.

are probably due to the frequent occurrence of dust storms in western India, countries such as Iran and Pakistan, and also in Arabian Peninsula. During these months many times the assumption of the rural aerosol model in INSAT-3D AOD algorithm does not hold good which results in large errors and low correlation coefficient. Except for March and December, the slope of regression line varies by 39% over unity. The comparison results over land show overall error of 27% in INSAT-3D AOD relative to MODIS-AOD excluding dust-contaminated months of March–April.

Figures 11a–11c show annual average map of MODIS-aqua AOD, INSAT-3D AOD, and the difference (INSAT-3D AOD − MODIS-aqua AOD), respectively, over Indian landmass and adjoining ocean. It is to be noted the both INSAT-3D and MODIS show high AOD features in entire IG plain and in coastal region. However, from the difference map it is evident that INSAT-3D AOD is mostly underestimated over Indian landmass, while over oceanic region most of the places the INSAT-3D are more or less in agreement with MODIS-aqua AOD.

5. Diurnal Variablity in INSAT-3D and AERONET AOD

Kaufman et al. (2000) reported that AOD may show systematic diurnal variability in regions with high anthropogenic and dust activities. Many of the AERONET sites situated in countries such as India and China included

Table 9
Same as Table 8 but Here Validation With Monthly Mean MODIS-Aqua AOD Over Indian Landmass at 1° Resolution

Month	*N*	*m*	*i*	*r*	σ_τ	Bias	$\langle\tau_{MODIS}\rangle$	$\langle\tau_{INSAT}\rangle$	$\sigma_\tau/\langle\tau_{MODIS}\rangle$
January	300	0.61	0.20	0.77	0.13	0.03	0.49	0.52	0.27
February	210	0.61	0.13	0.81	0.08	−0.05	0.52	0.47	0.15
March	139	0.58	0.23	0.52	0.16	0.01	0.52	0.53	0.31
April	111	0.98	0.13	0.45	0.30	0.16	0.39	0.55	0.77
May	116	0.77	0.16	0.81	0.13	0.05	0.52	0.57	0.25
June	55	0.73	0.30	0.89	0.12	0.19	0.51	0.70	0.24
September	25	0.89	0.03	0.82	0.14	−0.02	0.54	0.52	0.26
October	204	0.70	0.07	0.74	0.10	−0.05	0.43	0.38	0.23
November	230	0.70	0.02	0.88	0.08	−0.08	0.43	0.35	0.18
December	285	0.55	0.07	0.87	0.08	−0.06	0.33	0.28	0.24

Note. MODIS = Moderate Resolution Imaging Spectroradiometer; AOD = aerosol optical depth.

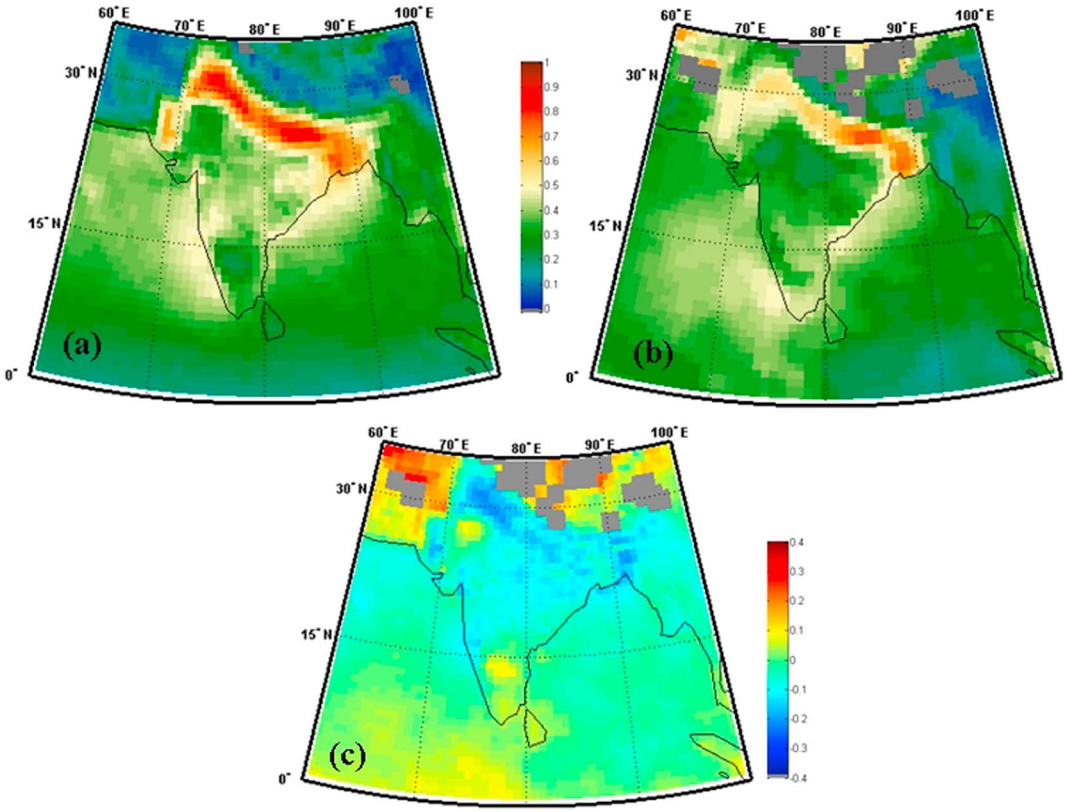

Figure 11. (a–c) Annual average map of MODIS-aqua AOD, INSAT-3D AOD, and the difference (INSAT-3D AOD − MODIS AOD), respectively, over Indian landmass and adjoining ocean. MODIS = Moderate Resolution Imaging Spectroradiometer; AOD = aerosol optical depth; INSAT-3D = Indian National Satellite.

in present study are highly affected by anthropogenic activities, and therefore, it will be very interesting to see the diurnal variability in INSAT-3D and AERONET AOD in these regions. To compare the diurnal trends in AOD, we identified all coincident INSAT-3D and AERONET AOD for the year 2016 based on criteria described in section 4.1. Then for each AERONET site, the mean of INSAT-3D and AERONET AOD at each retrieval time is calculated. The results are shown in Figures 12a and 12b. Figure 12a show results for stations located in China and Korean peninsula, whereas Figure 12b is for India and other Southeast Asian countries. The standard deviation of the mean is indicated by the error bars, while mean of AERONET AOD, INSAT-3D AOD, and the bias is shown by gray, red, and green bars, respectively. At sites located in China and Korian peninsula (Figure 12a) the diurnal trend in INSAT-3D AOD is in agreement with AERONET AOD with small bias varying between −0.1 and 0.1. At most of the sites INSAT-3D AOD shows negative bias. In general, all sites show gradually increasing AOD up to 0700 or 0730 UTC and then decreasing trend for both INSAT-3D and AERONET AOD with exception at site 9 (Chen_Kung_University) located in Taiwan.

In India and Southeast Asian countries (Figure 12b), the diurnal trend in the INSAT-3D AOD shows moderate to good agreement with AERONET AOD with large negative bias as compared to China and Korean peninsula. At some sites the bias significantly rises over −0.15. In Southeast Asia (site numbers 11, 12, and 13) interestingly it is found that INSAT-3D and AERONET AOD first decreases and then increases which is different from what is seen over China and Korean peninsula. On the other hand at sites located in IG plain (site numbers 14, 15, and 16) the AOD gradually increases from 0600 to 0830 UTC. The site numbers 17, 19, and 20 do not show significant diurnal change in AOD.

At many of the stations (Figures 12a and 12b it is evident that the bias is high near 0600 and 0830 UTC; however, this behavior cannot be confidently concluded because the time interval for which INSAT-3D retrivals are presented here only covers 3.5 hr (0600 to 0830 UTC) of the day in which scattering angle does not change significantly. The effect of small change in scattering angle on bias probably disappears in the uncertainty introduced by other factors responsible for bias.

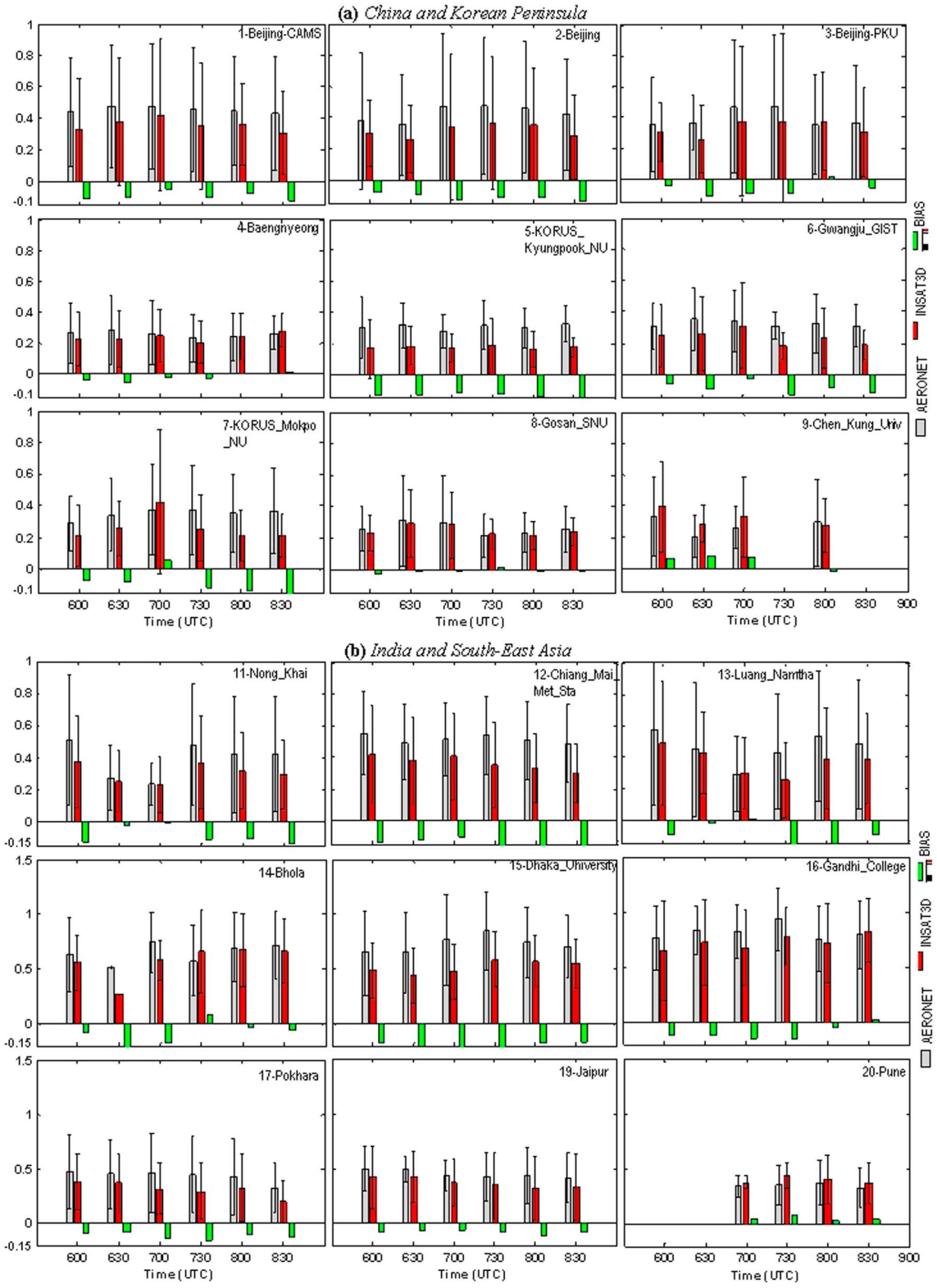

Figure 12. Comparison of the INSAT-3D (red bars) and AERONET (gray bars) AOD diurnal variability at various AERONET stations located over land. The bias in INSAT-3D AOD is shown in green bars. The vertical black lines show the standard deviation of AOD retrievals. INSAT-3D = Indian National Satellite; AERONET = Aerosol Robotic Network; AOD = aerosol optical depth.

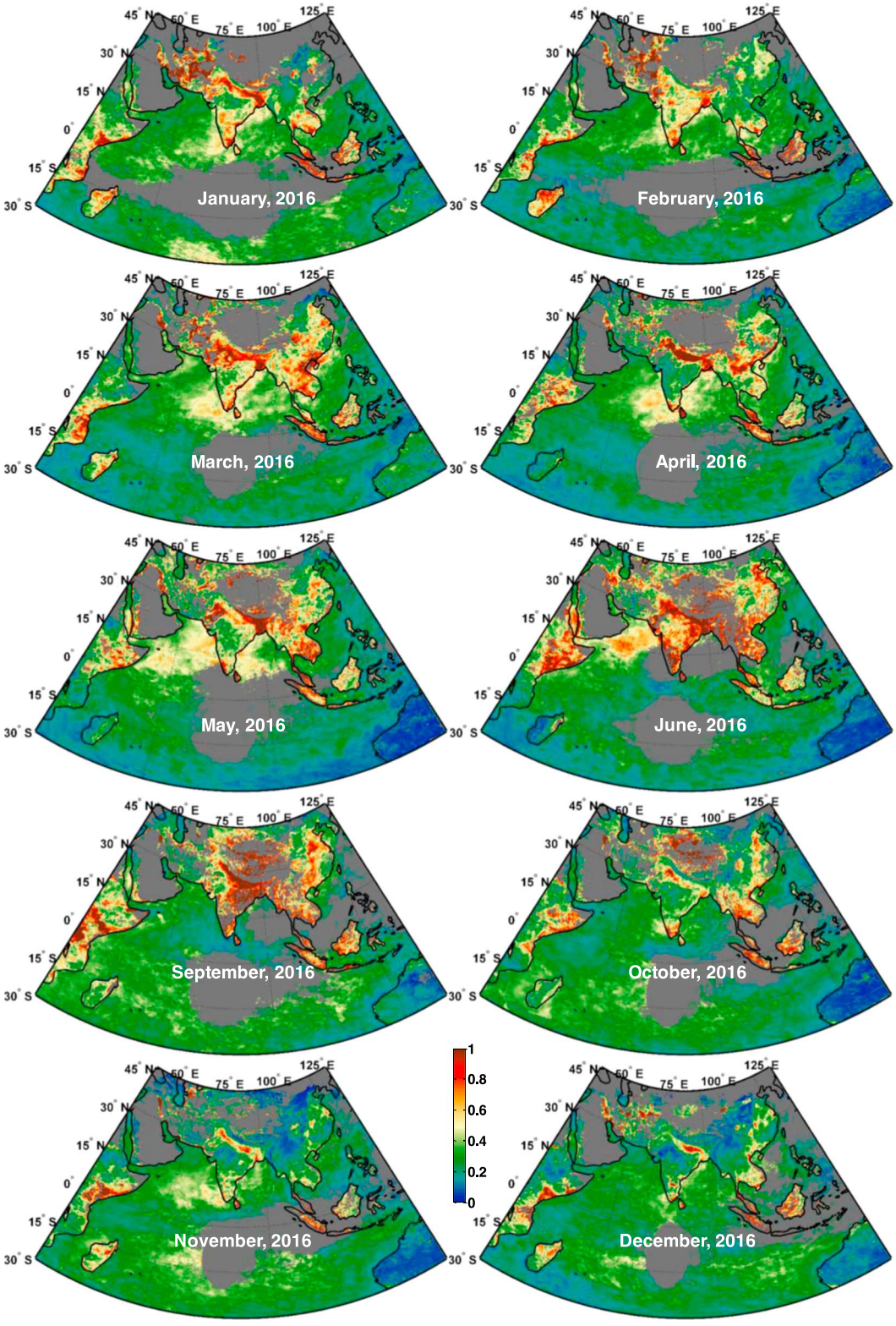

Figure 13. Climatological maps of monthly average of daily average INSAT-3D aerosol optical depth during the year of 2016. INSAT-3D = Indian National Satellite.

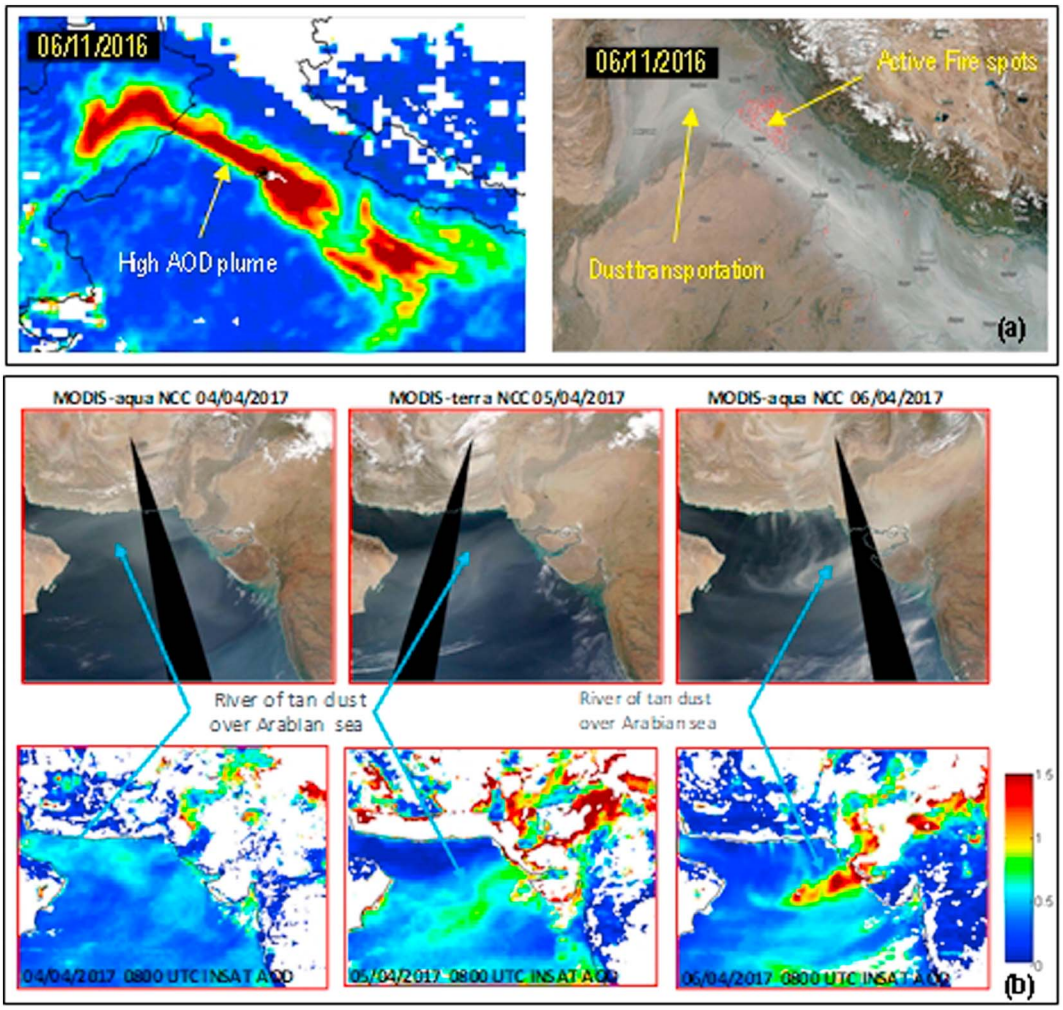

Figure 14. (a, b) The dust storm captured by INSAT-AOD product and MODIS on 6 November 2016 and during 4 to 6 April 2017. INSAT-3D = Indian National Satellite; AOD = aerosol optical depth; MODIS = Moderate Resolution Imaging Spectroradiometer.

6. INSAT-3D Aerosol Climatology

The monthly climatological maps of AOD using INSAT-3D AOD are generated. Figure 13 shows the monthly average state of AOD during 2016 over full INSAT-3D view coverage. Monthly averaged maps have been generated by averaging the daily averages of INSAT-3D AOD. While constructing the daily average maps, the INSAT-3D AOD retrieval from 0600 to 0830 UTC is used for the year 2016. Retrievals with satisfying conditions such as scattering angle are less than 160°; the number of observation greater than 15% of the days in month, glint-free over oceans, and 5 × 5 pixel window standard deviation lesser than 0.25 are only used. The maps in Figure 13 show consistent pollution over the IG plain in India over the year. The heavy pollution sources such as agriculture residue burning during October–November months in North-Indian states, biomass burning during winters (December-January-February), and transported dust during March, April, and May in addition to traffic and industrial pollution make such situation over the IG plain. In addition to these pollution sources, the low elevation of IG plain and the Himalayan range in North halts the transportation of the aerosols, resulting in a persistent thick layer of aerosol in this region. The monthly average maps of INSAT-3D AOD clearly show heavy pollution over China due to traffic and industrial pollution. It can be verified that the spatial distribution of aerosols observed by monthly climatology from various sensors such as MODIS-aqua and SeaWIFS is well captured by monthly average maps of INSAT-3D AOD shown here over both land and oceanic regions. Such climatological maps combined with aerosol information from other sources can be used in various application like aerosol radiative forcing and air quality status.

7. Dust Storm Monitoring From the INSAT-3D Aerosol Product

Figures 14a and 14b show the two dust storm events captured by MODIS-aqua true color images on 6 November 2016 and on 4–6 April 2017, respectively. The corresponding INSAT-3D AOD maps clearly show very high AOD plumes over regions covered by tanned dust. On 6 November 2016 the high AOD in IG plain was not only due to the transportation of dust resulted by the occurrence of dust storm event in Pakistan-Afghanistan border region (Figure 14a) but also due to the transportation of smoke by heavy burning of agriculture residue in Haryana and adjoining states of India as verified by MODIS-aqua active fire spots product (red dots in right panel of Figure 14a). Similarly, Figure 14b shows that dust storms occurred in Arabian Peninsula and in Iran/Pakistan region during 4–6 April 2017 led to the observation of wider stream of tanned dust over the Arabian Sea which is well captured by high AOD plume in INSAT-3D AOD maps on these days. Further INSAT-3D AOD maps show that this dust was transported to the Indian landmass (West Indian states and IG plain) on 5 and 6 April 2017, due to strong northeasterly blowing winds, thus decreasing air quality which is verified by sharp increase in INSAT-3D AOD and AERONET AOD ($>$1.0) over Jaipur and Kanpur on 6 April 2017. The high temporal resolution of INSAT-3D AOD product gives a slightly higher edge to the utility of INSAT-3D AOD product over MODIS and other AOD products in terms of close monitoring of transportation of dust due to strong dust storms occurring far away from the area of interest and understanding their impact on air quality.

8. Conclusion

In the present paper, currently operational algorithm developed to derive AOD from INSAT-3D Imager data is described and validated over Asian landmass and the Indian Ocean. The uncertainty analysis of INSAT-3D AOD retrievals under suitable atmospheric and surface conditions representative of INSAT-3D view coverage area is presented. The uncertainty analysis suggests an error of less than 30% and 45% over ocean and land regions, respectively, depending on the accuracy of assumed model parameters. Since in Asia certain regions such as IG plain, central and western India, and China show persistent hazy conditions due to high pollution (both anthropogenic and natural origin); therefore, MODIS AOD retrieval is used to generate climatological maps of background aerosol which is used in present algorithm to correct the CCIs to derive Lambertian surface reflectance.

The validation of INSAT-3D AOD against AERONET and handheld Sun-photometer aerosol retrievals shows that uncertainty of INSAT-3D AOD varies with geographical location with less uncertainty over dark surfaces such as ocean. The validation study at 22 AERONET stations shows high correlation coefficient ranging from 0.70 to 0.91 over land, except at four stations. The four stations, namely, Lahore (Pakistan), Kanpur (India), Gandhi college (India), and NGHIA_DO (Vietnam), are highly polluted areas due to anthropogenic activities. After analyzing the Parasol fine mode aerosol product and AERONET fine mode fraction over Lahore, Kanpur, and Gandhi college, it is found that the aerosols in these regions are dominated by fine aerosol particles which are significantly different from the assumed rural aerosol model used in the INSAT-3D AOD algorithm. Also, during winters from CALIOP observations, it can be verified that the mixed boundary layer in these regions decreases to 500 m, while in summers all of these regions are significantly affected by regional wind-blown dust as well as by dust transportation from dust storm frequently occurring in Arabian Peninsula, Afghanistan, Iran, and Pakistan regions. Therefore, the low correlation coefficient of INSAT-3D AOD with AERONET in these regions is primarily due to large uncertainty in assumed aerosol optical properties in retrieval algorithm. Retrieval errors over land are found to be less than 45% which is under theoretical uncertainty limit. Due to dark ocean surface, the retrieval errors, less than 30%, are observed over oceans with high correlation coefficient ranging from 0.79 to 0.91.

Comparison of monthly averaged AOD from MODIS and INSAT-3D shows good agreement. Excluding the dust-contaminated months October over oceans and March–April over landmass, both over oceans and Indian landmass high correlation ranging from 0.72 to 0.97 and 0.74 to 0.89, respectively, is found. Comparisons are well within the theoretical limits of uncertainty and thus shows the potential of INSAT-3D visible channel imagery to derive AOD. It is to be noted that MODIS aerosol retrievals are highly accurate and also give added information such as angstrom exponent and fine mode fraction, as MODIS algorithm uses observation from several narrow spectral channels ranging from visible to shortwave infrared wavelengths and dynamic aerosol models, whereas INSAT-3D AOD algorithm uses single broad visible channel

with static aerosol model (rural model over land and Maritime model for oceans) leading to significant uncertainties up to 45% and 30% over land and ocean surface, respectively.

The present validation shows that information about AOD from INSAT-3D and MODIS is comparable within the uncertainty limits and therefore can be combined to generate aerosol product at a high temporal resolution over Asian region to observe the dynamic changes in aerosol distribution and their sources over Asian region. The combined product may fill the gap of having AOD product at high temporal resolution over Asian landmass and adjoin oceans. Moreover, although INSAT-3D AOD is less accurate over land (up to 45% for some cases) than the MODIS, the high temporal resolution of INSAT observation makes INSAT-AOD product certainly a good option for close monitoring of dust transportation due to dust storms occurring far away from the area of interest. The present validation and uncertainty analysis also show that the uncertainty in INSAT-AOD retrievals can be decreased in future updates over land by selecting an appropriate set of spatially and temporally dynamic aerosol models based on ground observations such as AERONET and Aerosol Radiative Forcing in India Network and on other multispectral sensors that provide highly accurate aerosol information such as MODIS and Multiangle Imaging SpactroRadiometer, though at low temporal resolution.

Acknowledgments

We would like to acknowledge Prakash Chauhan for invaluable discussion and help in algorithm development. We would also like to thank Arundhati Misra, Rajkumar, and Shri Tapan Misra for their support. We also like to thank Principal Investigators (PIs) of AERONET stations for making their data available through AERONET website. We would also like to acknowledge Sahsikant Sharma and Pankaj Bodani for their support in operationalization of the algorithm on ISRO/VEDAS website (https://vedas.sac.gov.in/vedas/) from where data could be accessed by the users. We appreciate the reviewers for providing important suggestions to improve the manuscript. Although this work has been internally reviewed, the views and opinions expressed in this paper are those of the author and should not be interpreted as an official ISRO or Government of India position, policy, or decision.

References

Choi, M., Kim, J., Lee, J., Kim, M., Park, Y. J., Jeong, U., et al. (2016). GOCI Yonsei Aerosol Retrieval (YAER) algorithm and validation during DRAGON-NE Asia 2012 campaign. *Atmospheric Measurement Techniques*, *9*(3), 1377–1398. https://doi.org/10.5194/amt-9-1377-2016

d'Almeida, G. A., Koepke, P., & Shettle, E. P. (1991). *Atmospheric aerosols: Global climatology and radiative characteristics*. Hampton, VA: A. DEEPAK Publishing.

Dubovik, O., Holben, B., Eck, T. F., Smirnov, A., Kaufman, Y. J., King, M. D., et al. (2002). Variability of absorption and optical properties of key aerosol types observed in worldwide locations. *Journal of the Atmospheric Sciences*, *59*(3), 590–608. https://doi.org/10.1175/1520-0469(2002)059%3C0590:VOAAOP%3E2.0.CO;2

Hayasaka, T., Satake, S., Shimizu, A., Sugimoto, N., Matsui, I., Aoki, K., & Muraji, Y. (2007). Vertical distribution and optical properties of aerosols observed over Japan during the Atmospheric Brown Clouds-East Asia Regional Experiment 2005. *Journal of Geophysical Research*, *112*, D22S35. https://doi.org/10.1029/2006JD008086

Holben, B. N., Eck, T. F., Slutsker, I., Tanré, D., Buis, J. P., Setzer, A., et al. (1998). AERONET—A federated instrument network and data archive for aerosol characterization. *Remote Sensing of Environment*, *44*(1), 1–16.

Hsu, N. C., Jeong, M.-J., Bettenhausen, C., Sayer, A. M., Hansell, R., Seftor, C. S., et al. (2013). Enhanced deep blue aerosol retrieval algorithm: The second generation. *Journal of Geophysical Research: Atmospheres*, *118*, 9296–9315. https://doi.org/10.1002/jgrd.50712

Hsu, N. C., Tsay, S. C., King, M. D., & Herman, J. R. (2004). Aerosol properties over bright reflecting source regions. *IEEE Transactions on Geoscience and Remote Sensing*, *42*(3), 557–569. https://doi.org/10.1109/TGRS.2004.824067

Hsu, N. C., Tsay, S. C., King, M. D., & Herman, J. R. (2006). Deep blue retrievals of Asian aerosol properties during ACE-Asia. *IEEE Transactions on Geoscience and Remote Sensing*, *44*(11), 3180–3195. https://doi.org/10.1109/TGRS.2006.879540

Ichoku, C., Chu, D. A., Mattoo, S., Kaufman, Y. J., Remer, L. A., Tanre, D., et al. (2002). A spatio-temporal approach for global validation and analysis of MODIS aerosol products. *Geophysical Research Letters*, *29*(12), 8006. https://doi.org/10.1029/2001GL013206

INSAT-3D ATBD (2015). INSAT-3D algorithm theoretical basis development document, version 1, MOSDAC, Space Applications Centre, ISRO, Ahmedabad, India.

Intergovernmental Panel on Climate Change (2007). In S. Solomon, et al. (Eds.), *Climate change 2007: The physical science basis, contribution of working group I to the fourth assessment report of the intergovernmental panel on climate change*. Cambridge, United Kingdom and New York: Cambridge University Press.

ISRO-Geosphere-Biosphere Programme (2017). Proceedings of the project review meeting 2017: Aerosols and climate projects ARFI, ICARD, RAWEX & NOBLE, space physics laboratory, Vikram Sarabhai Space Centre, Indian Space Research Organization, Thiruvananthapuram, India.

Kaufman, Y. J., Holben, N., Tanre, D., Slutsker, I., Smirnov, A., & Eck, T. F. (2000). Will aerosol measurements from Terra and Aqua Polar Orbiting satellites represents the daily aerosol abundance and properties? *Geophysical Research Letters*, *27*(23), 3861–3864. https://doi.org/10.1029/2000GL011968

Kaufman, Y. J., Wald, A., Remer, L. A., Gao, B. C., Li, R. R., & Flynn, L. (1997). The MODIS 2.1-μm channel—Correlation with visible reflectance for use in remote sensing of aerosol. *IEEE Transactions on Geoscience and Remote Sensing*, *35*(5), 1286–1298. https://doi.org/10.1109/36.628795

Kim, J., Yoon, J., Ahn, M. H., Sohn, B. J., & Lim, H. S. (2008). Retrieving aerosol optical depth using visible and mid-IR channels from geostationary satellite, MTSAT-1R. *International Journal of Remote Sensing*, *29*(21), 6181–6192. https://doi.org/10.1080/01431160802175553

Kim, M., Kim, J., Wong, M. S., Yoon, J., Lee, J., Wu, D., et al. (2014). Improvement of aerosol optical depth retrieval over Hong Kong from a geostationary meteorological satellite using critical reflectance with background optical depth correction. *Remote Sensing of Environment*, *142*, 176–187. https://doi.org/10.1016/j.rse.2013.12.003

Knapp, K. R., Frouin, R., Kondragunta, S., & Prados, A. I. (2005). Towards aerosol optical depth retrievals over land from GOES visible radiances: Determining surface reflectance. *International Journal of Remote Sensing*, *26*(18), 4097–4116. https://doi.org/10.1080/01431160500099329

Knapp, K. R., Haar, T. H. V., & Kaufman, Y. J. (2002). Aerosol optical depth retrieval from GOES-8: Uncertainty study and retrieval validation over South America. *Journal of Geophysical Research*, *107*(D7), 4055. https://doi.org/10.1029/2001JD000505

Kolmonen, P., Sundstrom, A.-M., Sogacheva, L., Rodriguez, E., Virtanen, T., & de Leeuw, G. (2013). Uncertainty characterization of AOD for the AATSR dual and single view retrieval algorithms. *Atmospheric Measurement Techniques Discussions*, *6*(2), 4039–4075. https://doi.org/10.5194/amtd-6-4039-2013

Kotchenova, S. Y., & Vermote, E. F. (2007). Validation of a vector version of the 6S radiative transfer code for atmospheric correction of the satellite data. Part II: Homogeneous Lambertian and anisotropic surfaces. *Applied Optics*, *46*(20), 4455–4464. https://doi.org/10.1364/AO.46.004455

Kotchenova, S. Y., Vermote, E. F., Matarrese, R., & Klemm, F. J. Jr. (2006). Validation of a vector version of the 6S radiative transfer code for atmospheric correction of the satellite data. Part I: Path radiance. *Applied Optics*, *45*, 26, 6762–6774. https://doi.org/10.1364/AO.45.006762

Lenoble, J., & Brogniez, C (1984). A comparative review of radiation aerosol models. *Beitraege zur Physik der Atmosphaere*, *57*, 1–20.

Levy, R. C., Remer, L. A., Mattoo, S., Vermote, E. F., & Kaufman, Y. J. (2007). Second-generation operational algorithm: Retrieval of aerosol properties over land from inversion of Moderate Resolution Imaging Spectroradiometer spectral reflectance. *Journal of Geophysical Research*, *112*, D13211. https://doi.org/10.1029/2006JD007811

Li C., Xue, Y., Yang, L., & Guang, J. (2013). Uncertainties of aerosol retrieval from neglecting non-sphericity of dust aerosols. Geophysical Research Abstracts, 15, EGU2013–196-11.

Martins, J. V., Hobbs, P. V., Weiss, R. E., & Artaxo, P. (1998). Sphericity and morphology of smoke particles from biomass burning in Brazil. *Journal of Geophysical Research*, *103*(D24), 32,051–32,057. https://doi.org/10.1029/98JD01153

Martins, J. V., Tanré, D., Remer, L., Kaufman, Y., Mattoo, S., & Levy, R. (2002). MODIS cloud screening for remote sensing of aerosols over oceans using spatial variability. *Geophysical Research Letters*, *29*(12), 8009. https://doi.org/10.1029/2001GL013252

Patel, P. N., Bhatt, H., Mathur, A. K., Prajapati, R. P., & Tyagi, G. (2016). Reflectance-based vicarious calibration of INSAT-3D using high-reflectance ground target. *Remote Sensing Applications: Society and Environment*, *3*, 20–35. https://doi.org/10.1016/j.rsase.2015.12.001

Pope, C. A. III (2000). Epidemiology offine particulate air pollution and human health: Biologic mechanisms and who's at risk? *Environmental Health Perspectives*, *108*, 713–723. https://doi.org/10.2307/3454408

Prados, A. I., Kondragunta, S., Ciren, P., & Knapp, K. R. (2007). GOES Aerosol/Smoke Product (GASP) over North America: Comparisons to AERONET and MODIS observations. *Journal of Geophysical Research*, *112*, D15201. https://doi.org/10.1029/2006JD007968S

Vermote, E. F., Tanre, D., Deuze, J. L., Herman, M., & Morcrette, J. J. (1997). Second simulation of the satellite signal in the solar spectrum 6S: An overview. *IEEE Transactions on Gioscience and Remote Sensing*, *35*(3), 675–686. https://doi.org/10.1109/36.581987

Vermote, E. F., Tanre, D., Deuze, J. L., Herman, M, & Morcrette, J. J. (2006). Second simulation of the satellite signal in the solar spectrum–vector (6SV), 6S User Guide Version 3.

Wang, J., Christopher, S. A., Brechtel, F., Kim, J., Schmid, B., Redemann, J., et al. (2003). Geostationary satellite retrievals of aerosol optical thickness during ACE-Asia. *Journal of Geophysical Research*, *108*(D23), 8657. https://doi.org/10.1029/2003JD003580

Winker, D. M., Tackett, J. L., Getzewich, B. J., Liu, Z., Vaughan, M. A., & Rogers, R. R. (2013). The global 3-D distribution of tropospheric aerosols as characterized by bCALIOP. *Atmospheric Chemistry and Physics*, *13*(6), 3345–3361. https://doi.org/10.5194/acp-13-3345-2013

WMO-WCP112 (1986). World Climate Programme: A preliminary cloudless standard atmosphere for radiation computation, World Meteorological Organization, WMO/TD-No 24, Geneva.

Zhang, H., Lyapustin, A., Wang, Y., Kondragunta, S., Laszlo, I., Ciren, P., & Hoff, R. M. (2011). A multi-angle aerosol optical depth retrieval algorithm for geostationary satellite data over the United States. *Atmospheric Chemistry and Physics*, *11*(11977–11991), 2011. https://doi.org/10.5194/acp-11-11977-201